

# Sommerfeld Effect for a Rotor with Axisymmetric Support Stiffness

A Major Qualifying Project

submitted to the Faculty of the

WORCESTER POLYTECHNIC INSTITUTE

in partial fulfillment of the requirements for the Degree of Bachelor of Science

---

by : Jiaxun Xie

Mechanical Engineering and Mathematical Sciences

Class of 2016

---

Advisor: Professor Mikhail Dimentberg

Professor Burt Tilley

This report represents the work of WPI undergraduate students submitted to the faculty as evidence of completion of a degree requirement. WPI routinely publishes these reports on its website without editorial or peer review. For more information about the projects program at WPI, please see <http://www.wpi.edu/academics/ugradstudies/project-learning.html>

# Contents

<b>Executive Summary</b>	<b>5</b>
<b>1 Introduction</b>	<b>6</b>
Background . . . . .	6
Literature Review . . . . .	7
<b>2 Methodology</b>	<b>14</b>
Analytical Method (Krylov-Bogoliubov Averaging Method) . . . . .	14
Computational Technique (Runge-Kutta-Fehlberg) . . . . .	16
<b>3 Formulation</b>	<b>21</b>
Non-Dimensionalization . . . . .	22
<b>4 Steady-state Response</b>	<b>24</b>
<b>5 Transient Response</b>	<b>29</b>
Stability of steady-state response . . . . .	33
<b>6 Numerical Simulation</b>	<b>37</b>
Passage/Capture . . . . .	37
Three cases of motor torque . . . . .	42
Results . . . . .	47
Validation of Steady-state Case . . . . .	47
Passage Technique for Axisymmetric Case . . . . .	49
a. Passage on $x$ -displacement but capture on $y$ -displacement . . . . .	50
b. Passage on both $x$ -displacement and $y$ -displacement . . . . .	50
c. Comparison . . . . .	51
<b>7 Conclusion</b>	<b>55</b>

<b>8 Appendices</b>	<b>57</b>
Appendix A: Table of analytical steady-state torque $\bar{M}_{ss}$ and numerical steady-state torque $M_*$ at $\nu = 1$ and $\nu = \Omega$ . . . . .	57
Appendix B: Matlab codes . . . . .	58
a. Equations of system . . . . .	58
b. Runge-Kutta-Fehlberg method . . . . .	59
c. Simulation by RKF . . . . .	61

# List of Figures

1	(1D) model . . . . .	7
2	(1D) Steady-state values of the rotational frequency . . . . .	8
3	(1D) Displacement and Angular Velocity vs. Time of slow passage . . . . .	10
4	(2D) Model of system . . . . .	21
5	(2D) Steady-state curve $\bar{M}_{ss}$ vs. $\nu$ . . . . .	26
6	(2D) Steady-state torque at $\nu = 1$ , $(\bar{M}_{ss})_1$ vs. $\Omega$ . . . . .	27
7	(2D) Steady-state curve at $\nu = \Omega$ , $(\bar{M}_{ss})_2$ vs. $\nu$ . . . . .	28
8	(2D) Stability indicator $\beta$ vs. angular velocity $\nu$ with different $\Omega$ . . . . .	35
9	(2D) Steady-state curve $\bar{M}_{ss}$ vs. $\nu$ (with stability) . . . . .	36
10	(2D) Passage . . . . .	39
11	(2D) Capture . . . . .	40
12	(2D) Slow-passage . . . . .	41
13	(2D) Vibration with motor torque above both $(\bar{M}_{ss})_1$ and $(\bar{M}_{ss})_2$ . . . . .	44
14	(2D) Vibration with motor torque between $(\bar{M}_{ss})_1$ and $(\bar{M}_{ss})_2$ . . . . .	45
15	(2D) vibration with motor torque below $(\bar{M}_{ss})_1$ and $(\bar{M}_{ss})_2$ . . . . .	46
16	(2D) Stability of steady-state torque curve $\bar{M}_{ss}$ vs. angular velocity $\nu$ . . . . .	47
17	(2D) Numerical stability of steady-state torque curve $\bar{M}_{ss}$ vs. angular velocity $\nu$ . . . . .	48
18	(2D) Comparison between $(\bar{M}_{ss})_1$ and $(M_*)_1$ . . . . .	51
19	(2D) Comparison between $(\bar{M}_{ss})_2$ and $(M_*)_2$ . . . . .	52
20	(2D) Comparison between $(\bar{M}_{ss})_1$ and $(\bar{M}_{ss})_2$ . . . . .	53
21	(2D) Comparison between $(M_*)_1$ and $(M_*)_2$ . . . . .	53

# Executive Summary

Sommerfeld effect is a common phenomenon for unbalanced rotating shaft excited by a limited power supply. When the power supply is not sufficient for vibration to pass over the resonance, the shaft will slow down or be captured at resonance. Analyses of the phenomenon are conducted for shaft with axisymmetric stiffness and for the case where the vibration is one-dimensional due to imposed constraints. The goal of this project is to fill the gap between the above two extreme cases of two-dimensional vibration system with two spring sets attached to the unbalanced shaft. The axisymmetric case denotes the asymmetry in spring stiffness, while the one-dimensional case corresponds to one of the spring set has infinite stiffness acting as the constraint.

Krylov-Bogoliubov averaging method was used to access the analytical motor torque for steady-state response, which is the lowest motor torque required for passage over resonance. The stability criteria of steady-state torque were considered as well. Transient case provides the information of vibration that is approaching its steady state. Runge-Kutta-Fehlberg method was used in numerical simulation to validate the steady-state torque with its stability criteria. By considering the analytical steady-state torque at two specific points of rotation speed,  $\nu = 1$  and  $\nu = \Omega$ , a passage technique for axisymmetric vibration system was introduced. The technique was validated by Runge-Kutta-Fehlberg method. The passage technique applies to two-dimensional vibration system with asymmetric spring stiffness. With the power supply that initially causes capture at x-vibration and y-vibration, the rotating shaft will passage over both x- and y-resonances by slightly raising one of the spring stiffness. This technique reduces the required power supply for rotation machine to pass over resonance. The analysis of steady-state response and transient response of two-dimensional vibrations fills in the gap between the axisymmetric case and one-dimensional case. It provides a more comprehensive study of two-dimensional systems.

# 1 Introduction

## Background

Motors are a commonly used component in plants and machinery. The shaft of the motor is not always balanced, and the small unbalance of the mass can cause lateral vibration of the system. The vibration caused by rotation can determine the machine life, because the foundation holding the plants has to support the vibration, and excessive vibration may destroy and even ruin the plants. In 1902, German theoretical physicist, Arnold Sommerfeld, discovered an energy sink at resonance of equipment generating with an unbalanced motor, in Sommerfeld et al. [1], Dimentberg et al. [3], Samantaray et al. [7]. The energy sink is a phenomenon that the vibration is captured at resonance with a large amplitude, so that the major part of the power supply is diverted to vibrate the structure, instead of increasing the rotation velocity. This phenomenon was later named as the Sommerfeld effect.

The Sommerfeld effect occurs with unbalanced shaft equipment. Studying the system with an unbalanced shaft can predict the threshold value for driving torque that will exclude the capture at resonance, so that the rotation speed increases without being captured at a constant value, and the vibration amplitudes return to a smaller value from resonance amplitude. In the previous century, the Sommerfeld effect has been widely seen in mechanical engineering applications in Dimentberg et al. [3], Segalman et al. [4], Cveticanin et al. [6], Samantaray et al. [7], and aerospace engineering applications in Kinsey et al. [2], Tsui et al. [8]. Techniques of passage over resonance with a limited power supply were invented to prevent the unwanted vibration, in order to extend machine life, Dimentberg et al. [3], Segalman et al. [4], Kononenko et al. [5]. In Aerospace Engineering, the effect of capture at resonance had been experienced for dual-spin spacecraft, Tsui et al. [8]. This problem was further solved by a nonlinear controller to reduce resonance during the spin through precession phase lock, Kinsey et al. [2].

In previous research, Sommerfeld effect has been considered in the one-dimensional case, that the vibration caused by rotation is constrained in linear motion, in Sommerfeld et al. [1], Dimentberg et al. [3], Kononenko et al. [5], Cventicanin et al. [6], and Bolla et al. [10]. As in applications, the constraints used to achieve one-dimensional vibration are connected to the foundation of the equipment, assuming the material of constraints has infinite stiffness. But even with an extremely high value of stiffness, there still occurs two-dimensional vibrations in the system. Studying two-dimensional vibrations can also lead to inventions of more techniques of passage over Sommerfeld effect.

## Literature Review

Consider a one-dimensional vibration motivated by an unbalanced shaft, with interaction of motor by a limited power supply. Figure (1) is the plot of the system, Dimentberg et al. [3]. Two constraints in shaded area are used to maintain the vibration in linear motion, and on  $x$ -axis, a spring set is considered as the foundation of the plant. The unbalanced mass  $m_1$  is attached on the rotating shaft with offset  $r$ . The governing

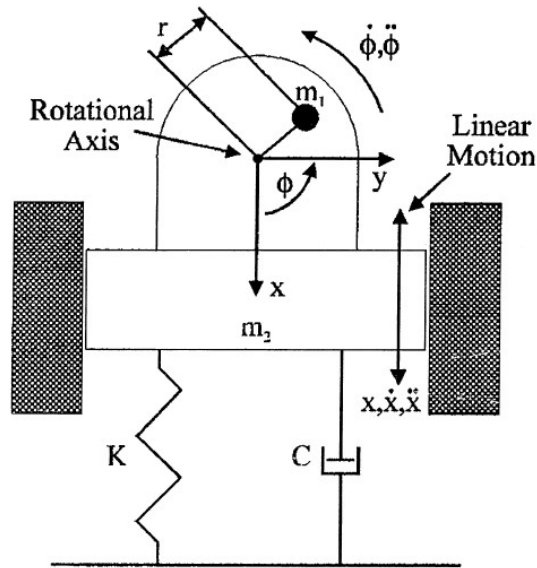


Figure 1: Model of an unbalanced rotating shaft on a movable support with elastic suspension spring;  $x(t)$  and  $\phi(t)$  are translational displacement and rotation angle of the shaft, respectively. Dimentberg et al. [3]

differential equations of the system are given by:

$$m_2\ddot{x} + C\dot{x} + Kx = m_1r\dot{\phi}^2 \cos \phi + m_1r\ddot{\phi} \sin \phi , \quad (1)$$

$$I\ddot{\phi} = L(\dot{\phi}) - R(\dot{\phi}) + m_1r\ddot{x} \sin \phi + m_1gr \cos(\phi + \frac{\pi}{2}) . \quad (2)$$

where  $m_1$  is the unbalanced mass of motor,  $m_2$  is the mass of vibrator,  $C$  is the damping coefficient,  $K$  is the spring stiffness,  $r$  is the offset of the unbalanced mass, and  $g$  is the gravitational acceleration. As shown in Figure 1,  $x(t)$  is the function of translational displacement depending on time  $t$ ,  $\phi(x)$  is the function of rotation angle.  $I$  denotes the shaft's mass moment of inertia.  $L(\dot{\phi})$  is the driving torque of the motor, and  $R(\dot{\phi})$  is the resisting torque. These are prescribed functions of the motor properties.

Figure (2) illustrates the steady-state value of the rotational frequency satisfying Eq.(1), for three different cases of the available torque-speed characteristic  $L$  curve, Dimentberg et al. [3].  $S$  curve is the apparent resistance torque derived from the resisting torque function  $R$ . The dashed part of  $S$  curve corresponds to the unstable case. The intersections of the  $L$  curves and  $S$  curve are steady-state values of rotational frequency. From this figure, curve  $L(1)$  has only one steady-state frequency, which means in this

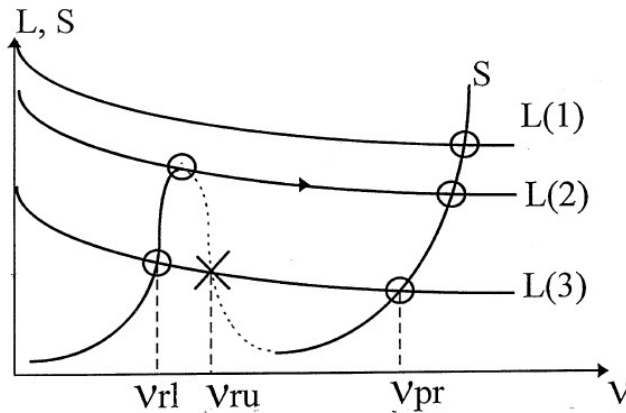


Figure 2: Graphical illustration of constant steady-state values of the rotational frequency, for three different cases of the available torque-speed curve  $L$  (labelled according to the number of the roots of the equation). Unstable part of the  $S$  curve is indicated by a dashed line for the case where  $L$ -curves form an equidistant set. Curve  $L2$  corresponds to the borderline case between those with a single value of the frequency and with three such values. It also controls slow or quasistatic passage through resonance, as indicated by an arrow. Dimentberg et al. [3]

case, the shaft always passes through resonance, although some slowdown is possible. On curve  $L(2)$ , there are two roots for steady-state frequency. The one at the peak of the  $S$  curve is unstable, so it jumps to another stable steady-state point; this is called jump phenomenon.  $L(2)$  is a borderline between the single value of frequency, like  $L(1)$ , and three values of frequency,  $L(3)$ .

Numerical methods are generally required in the study of transient motions, since analytical methods are only applicable to cases under specific conditions. The paper Dimentberg et al. [3] obtained the numerical solution, as well as extensive parametric studies.

The one-dimensional problem considered in Dimentberg et al. [3] is a typical problem of system with the non-ideal energy source. The rotation of motor is excited by energy source. Non-ideal system is a vibrating system for which the power supply is limited. Rotor dynamic systems are often analyzed with ideal motor drive assumption. This assumption can simplify the problem; however, it is only applicable in the following two cases. One case is when the operating range of the system is so limited, that there is sufficient power available from the drive. Another case is when the drive remains uninfluenced by the systems vibration, so that it can be approximated as an ideal motor drive.

Non-ideal power supply has the property, that there exists an interaction between the vibrator and motor. This interaction is always nonlinear, due to the trigonometric function of rotation angle, affecting the vibrations in Cartesian coordinates. Therefore, to deal with non-ideal power supply, one additional equation Eq.(2), describing the interaction between motor and vibrator, has to be added to the governing differential equation of the system Eq.(1).

When the available power of the drive is comparable with power consumption due to vibration, various nonlinear phenomena may be observed, which corresponds to the Sommerfeld effect. In numerous engineering applications, an increase of available driving

power is used to pass over the resonance; but when the additional power consumption due to vibration is comparable with the limited power of the driving motor, this approach may become impractical because of Sommerfeld effect. Therefore, some examples of techniques of passage with limited power supply are the method of changing stiffness by removing the originally additional stiffness, Dimentberg et al. [3], and switching stiffness by using shape memory alloys, Segalman et al. [4], Kononenko et al. [5].

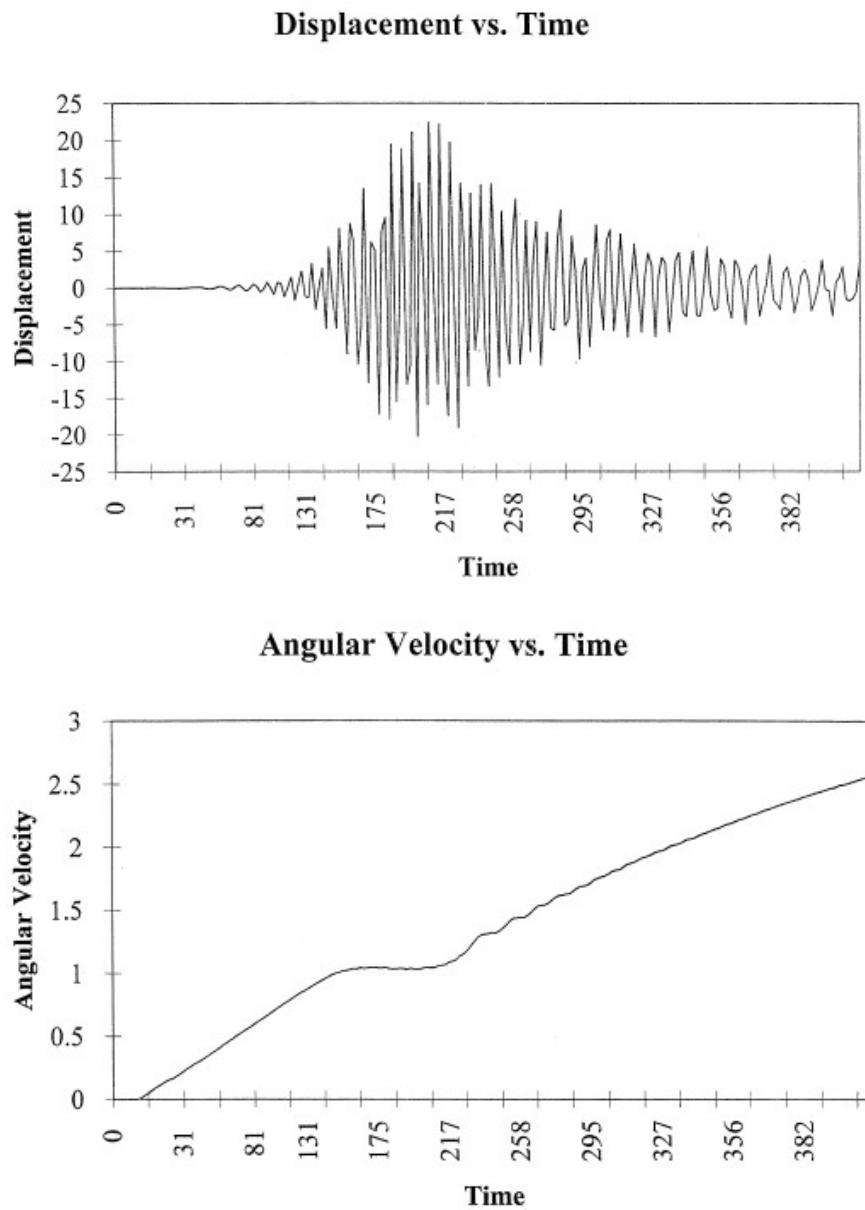


Figure 3: Displacement responses (upper traces) and shaft angular frequencies (lower traces) vs. time, as obtained by numerical simulation in search of a passage/capture threshold for the case of a passage with slowdown with 30% of the quasistatic threshold. Dimentberg et al. [3]

Figure 3 from Dimentberg et al. [3], are plots of displacement and angular velocity of one-dimensional vibration passing through resonance. The amplitude increases when the vibration is getting close to resonance, and reaches maximum at resonance. During the passage, the angular velocity slows down temporarily. After the resonance is passed over, the amplitude decreases, and the angular velocity grows again. Different from capture at resonance, the passage over resonance reflects that the vibration is reduced, and the power supply continues to accelerate the rotation speed.

The two-dimensional vibration problems can contain nonlinear terms. Nonlinearity comes from the interaction between vibrator and motor, due to the non-ideal energy source, nonlinear motor torque, and nonlinear elastic force. The nonlinear interaction of non-ideal energy source is not negligible unless in the case of an unlimited power supply. In general, the torque of the electro-motor, which is the net torque by deducting resisting torques from driving torques, is assumed to be linear. This torque is the characteristic of motors. A previous research of DC motors, asynchronous and synchronous motor, proved that the motor torques are commonly nonlinear Kononenko et al. [5]. In this report, we assume that the motor torque is from a lossless power supply, so that the motor torques are constant values.

The elastic force, modeled as a spring stiffness, can also be a nonlinear function. An electromotor with an unbalance is connected to a visco-elastic structure with nonlinear properties. Nonlinear spring stiffness is common in a significant number of materials, for example, aluminum, titanium and other aircraft materials, Prathap et al. [11], copper and copper alloys, Lo et al. [12], ceramic materials, Colm et al. [13] show nonlinear stress-strain properties of the material. The nonlinear dependence of the restoring force on the deflection is a polynomial whose exponent is of positive integer or non-integer order. For most materials, the damping properties are also nonlinear, but since the order of nonlinearity in the damping force is small, linear damping force model can be used as a good approximation. A detailed explanation of nonlinearity involved in the problem

can be found in the paper Cveticanin et al. [6].

We only consider linear spring stiffness in this report.

Perturbation theory is a method to find an approximate solution to a problem by starting from the exact solution of a related while simpler problem, and then adding the perturbation series in small parameter, Verhulst et al. [9]. Krylov-Bogoluiboy averaging method replaces the exact differential equation of the motion by its averaged version. For two or more timescales, the long time scales are assumed to be independent of the short time scales, which requires the condition that guarantees variations in slow vector solution within the period of variations in the fast time scale. The detailed explanation and process of applying this method is included in the paper, Verhulst et al. [9].

Krylov-Bogoluiboy averaging method is a commonly used method to deal with problems of oscillating processes in nonlinear mechanics. The application of Krylov-Bogoluiboy averaging method can be found in the papers Dimentberg et al. [3], Verhulst et al. [9], Bolla et al. [10]. In our research, we decided to apply Krylov-Bogoluiboy method to solve for analytic results.

Numerical simulation is used to validate the analytic results and also can be used to explore the transient effects in passage through resonance. Analytic results by applying Krylov-Bogoluiboy averaging method can only be found under specific conditions in our problem: small damping, small unbalance and small difference between the natural frequencies. And it is for the steady-state response. Thus numerical simulation can analyze the general case without the conditions of small values, and consider the transient cases.

Runge-Kutta method is a commonly used method for numerical simulation of Sommerfeld effect problems. The applications of Runge-Kutta method can be found in the papers Dimentberg et al. [3], Cveticanin et al. [6], Samantaray et al. [7].

Runge-Kutta-Fehlberg is an updated method under Runge-Kutta family, which is also called as Runge-Kutta45 method, Burden et al. [17]. Different from Runge-Kutta

method, which has uniform step size, Runge-Kutta-Fehlberg has step size that is adaptive to the number and position of the grid points. The idea of the method is to begin with two Runge-Kutta approximations, with order 4 and order 5. Then apply the algorithms to get two approximations at a given grid point. If the error approximation at the grid point exceeds some prescribed maximum bound on accuracy, a smaller step size is assigned as well as a new grid point, then repeat the steps for further points. If the error approximation falls below the present minimum bound on accuracy, which indicates a good approximation, the step size will increase for the next step. If the error approximation falls in between the maximum and minimum bounds, the step size will remain constant for proceeding steps.

In this report, we consider a two-dimensional vibrations system with two spring sets in vertical and horizontal axes. The one-dimensional vibrating system can be considered as a two-dimensional system with one of the spring set has infinite stiffness, i.e. the ratio of stiffnesses is infinity. The other extreme case of two-dimensional vibrations is axisymmetric case, which the stiffnesses of two spring sets are equal, i.e. the ratio of stiffnesses is unity. The case of axisymmetric shaft has been solved by Kononenko in his book, Kononenko et al. [18]. The goal of the project is to fill in the gap between the above two extreme cases. The model with its equation of system is demonstrated in Chapter 3. In Chapter 4 and 5, we use Krylov-Bogoliubov averaging method for analytical analysis of steady-state reponse and transient reponse. Moreover, we consider the stability criteria of the steady state reponse. Detailed numerical simulations on the transient reponse, and the results are stated in Chapter 6.

## 2 Methodology

### Analytical Method (Krylov-Bogoliubov Averaging Method)

The basic idea of averaging method can be dated back to the late 18th century, when Lagrange formulated the gravitational three-body problem as a perturbation of the two-body problem in 1788. In 1930s, the averaging method became one of the classical methods for approximate analysis of oscillating processes in non-linear mechanics. The method is named after Nikolay Krylov and Nikolay Bogoliubov.

Averaging method is applicable to systems of the form:

$$\dot{x} = \epsilon X(x, t); \quad \epsilon \ll 1 . \quad (3)$$

Here matrix  $X(x, t)$  is periodic with period  $T$  in explicitly present time  $t$ . Therefore it can be expanded in complex Fourier series as:

$$X(x, t) = \sum_{k=-\infty}^{k=\infty} X_k(x) \exp(ik\nu t) . \quad (4)$$

where  $\nu = 2\pi/T$ ,  $X_k(x) = \frac{1}{T} \int_0^T X(x, t) \exp(-ik\nu t) dt$ .

With  $\epsilon \rightarrow 0$ , solution to the matrix ODE (3) satisfies  $x(t) \rightarrow x_0(t)$ .  $x_0(t)$  is the solution vector to the matrix ODE with the RHS containing only the term of  $k = 0$  in the series (4):

$$\dot{x}_0 = \epsilon X_0(x_0); \quad \text{where } X_0(x) = \frac{1}{T} \int_0^T X(x, t) dt . \quad (5)$$

As an example, from Verhulst [9].

$$\ddot{x} + \epsilon(2 - e^{-\epsilon t})\dot{x} + x = 0 . \quad (6)$$

Introducing  $\tau = \epsilon t$ , along with the regular perturbation expansion  $x = x_0 + \epsilon x_1 + \epsilon^2 + \dots$ ,

and expansion of the Eq.(6) yields

$$\begin{aligned} & \left( \frac{\partial^2}{\partial t^2} + 2\epsilon \frac{\partial^2}{\partial t \partial \tau} + \epsilon^2 \frac{\partial^2}{\partial t^2} + \epsilon^2 + \dots \right) (x_0 + \epsilon x_1 + \epsilon^2 + \dots) \\ & + \epsilon(2 - e^{-\tau}) \left( \frac{\partial}{\partial t} + \epsilon \frac{\partial}{\partial \tau} \right) (x_0 + \epsilon x_1 + \epsilon^2 + \dots) + (x_0 + \epsilon x_1 + \epsilon^2 + \dots) = 0 . \end{aligned} \quad (7)$$

Colleting the terms of the order  $\epsilon$ , we find the equation to zero order

$$\frac{\partial^2 x_0}{\partial t^2} + x_0 = 0 . \quad (8)$$

The general solution of Eq. (8) is  $x_0(t, \tau) = A(\tau) \cos t + B(\tau) \sin t$ .

Transform  $x, \dot{x} \rightarrow A, B$  by variation of parameters. In this problem, dot denotes derivative with respect to  $t$ , for example  $\dot{x} = \frac{dx}{dt}$ . Taking the derivative with respect to  $t$  of  $x$ , we get  $\dot{x} = -A \sin t + B \cos t + \dot{A} \cos t + \dot{B} \sin t$ . By variation of parameters, let  $\dot{A} \cos t + \dot{B} \sin t = 0$ , so that

$$\dot{x} = -A \sin t + B \cos t , \quad (9)$$

then

$$\ddot{x} = -\dot{A} \sin t + \dot{B} \cos t - A \cos t - B \sin t . \quad (10)$$

Substituting Eq (9) and (10) into the equation of system Eq. (6):

$$-\dot{A} \sin t + \dot{B} \cos t + \epsilon(2 - e^{-\epsilon t})(-A \sin t + B \cos t) = 0 . \quad (11)$$

Use Eq (11) and the condition for variation of parameters,  $\dot{A} \cos t + \dot{B} \sin t = 0$ , to solve for  $\dot{A}$  and  $\dot{B}$ :

$$\dot{A} = \frac{dA}{dt} = \epsilon \frac{dA}{d\tau} = \epsilon(2 - e^{-\tau})(-A \sin t + B \cos t) \sin t , \quad (12)$$

$$\dot{B} = \frac{dB}{dt} = \epsilon \frac{dB}{d\tau} = -\epsilon(2 - e^{-\tau})(-A \sin t + B \cos t) \cos t , \quad (13)$$

as  $\tau = \epsilon t$ .

Both sides of Eq.(12) are the order  $\epsilon$ , so that we can apply the averaging method for Eq.(12):

$$\int_0^{2\pi} \frac{dA}{d\tau} dt = \int_0^{2\pi} (2 - e^{-\tau})(-A \sin^2 t + B \sin t \cos t) dt , \quad (14)$$

$$2\pi \frac{dA}{d\tau} = (2 - e^{-\tau})(-A\pi + 0) , \quad (15)$$

$$\frac{dA}{d\tau} = -\frac{1}{2}(2 - e^{-\tau})A . \quad (16)$$

Similarly, for Eq. (13):

$$\int_0^{2\pi} \frac{dB}{d\tau} dt = \int_0^{2\pi} (2 - e^{-\tau})(-A \sin t \cos t + B \cos^2 t) dt , \quad (17)$$

$$\frac{dB}{d\tau} = -\frac{1}{2}(2 - e^{-\tau})B . \quad (18)$$

So that the first order for  $x(t)$ :

$$x_0 = \exp\left(-\tau - \frac{1}{\exp(-\tau)}\right) (A(0) \cos t + B(0) \sin t) . \quad (19)$$

where  $A(0)$  and  $B(0)$  are determined by the initial conditions.

## Computational Technique (Runge-Kutta-Fehlberg)

*Runge-Kutta* methods belong to a family of increasingly accurate, and time-efficient methods, named after two German scientists: Carl Runge (1856-1927), mathematician and physicist, and Martin Kutta (1867-1994), mathematician. Generalized from Modified Euler and Midpoint methods, the methods of higher order with global error of  $O(h^k)$  with  $k \geq 3$ . *Runge-Kutta-Fehlberg* method adapts the number and position of the grid points during the course of the iteration in attempt to keep the local error within some specified bound.

The derivation of 2-stage Runge-Kutta scheme is the characteristic of the higher order

Runge-Kutta methods. The general form of an explicit two-stage Runge-Kutta Method is

$$\begin{aligned}x_{i+1} &= x_i + h(\alpha k_1 + \beta k_2) , \\k_1 &= f(t_i, x_i) , \\k_2 &= f(t_i + ah, x_i + ahk_1) .\end{aligned}$$

where  $dx/dt = f(t, x)$ . Two example methods that fit this pattern are midpoint method ( $a = 1/2, \alpha = 0, \beta = 1$ ) and Heun's Method ( $a = 1, \alpha = \beta = 1/2$ ), both have approximation with error no greater than  $O(h^2)$ . To estimate the local truncation error of these methods, perform the Taylor expansions of the terms of the general 2-stage Runge-Kutta Methods. Substituting  $k_1$  in the definition of  $k_2$ ,

$$k_2 = f(t_i + ah, x_i + ahf(t_i, x_i)) . \quad (20)$$

Since  $f'(t, x) = \frac{df}{dt}(t, x) = \frac{\partial f}{\partial t}(t, x) + \frac{\partial f}{\partial x}(t, x) \cdot x'(t)$ , and  $x'(t) = f(t, x)$ , we have

$$k_2 = f(t_i, x_i) + ah \frac{\partial f}{\partial t}(t_i, x_i) + ah \frac{\partial f}{\partial x}(t_i, x_i) \cdot f(t_i, x_i) + O(h^2) . \quad (21)$$

When this is inserted in the expression for  $x_{i+1}$ , we find

$$x_{i+1} = x_i + h(\alpha + \beta)f(t_i, x_i) + \frac{h^2}{2}2a\beta \left[ \frac{\partial f}{\partial t}(t_i, x_i) + \frac{\partial f}{\partial x}(t_i, x_i) \cdot f(t_i, x_i) \right] + O(h^3) . \quad (22)$$

Comparing this to Taylor series, we can see the conditions for the expansion (22) to match the first two terms of Taylor series

$$x(t_{i+1}) = x(t_i) + hx'(t_i) + \frac{h^2}{2}x''(t_i) + O(h^3) , \quad (23)$$

are

$$\alpha + \beta = 1 , \quad (24)$$

$$2a\beta = 1 . \quad (25)$$

It is straightforward to check that the midpoint method and the Heun's Method satisfy these conditions.

The outline of *Runge-Kutta-Fehlberg* algorithm can be found in the following steps. Begin with two RK approximation algorithms, one with order  $p$  and with order  $p + 1$ ; we used  $p = 4$ . Apply 4th-order-RK and 5th-order-RK to get two approximations at a given grid point  $t_1$ . The approximations are used to approximate the local error at the grid point. If the error of 4th-order-RK is within the prescribed tolerance, then the preceding process is repeated with 4-order algorithm. If the error approximation exceeds some prescribed maximum bound on accuracy, a smaller step size is assigned, and a new grid point is used. The preceding steps are repeated; the two RK approximations will be recomputed using the new grid point. If the error is between the minimum and maximum bounds, the approximation is acceptable, so the acceptable step size can be used to advance to the next grid point. If the error is lower than the minimum bound, the step size is more than adequate, and will be increased until it reaches maximum bound.

In an interval  $[a, b]$ , with initial values  $x_0$ , we calculate

$$\begin{aligned} k_1 &= hf(t_i, x_i) , \\ k_2 &= hf\left(t_i + \frac{h}{4}, x_i + \frac{1}{4}k_1\right) , \\ k_3 &= hf\left(t_i + \frac{3}{8}h, x_i + \frac{3}{32}k_1 + \frac{9}{32}k_2\right) , \\ k_4 &= hf\left(t_i + \frac{12}{13}h, x_i + \frac{1932}{2197}k_1 - \frac{7200}{2197}k_2 + \frac{7296}{2197}k_3\right) , \\ k_5 &= hf\left(t_i + h, x_i - \frac{429}{216}k_1 - 8k_2 + \frac{3680}{513}k_3 - \frac{845}{4104}k_4\right) , \\ k_6 &= hf\left(t_i + \frac{h}{2}, y_i - \frac{8}{27}k_1 + 2k_2 - \frac{3544}{2465}k_3 + \frac{1859}{4104}k_4 - \frac{11}{40}k_5\right) ; \end{aligned}$$

$$\begin{aligned}
x_{i+1} &= x_i + \frac{25}{216}k_1 + \frac{1408}{2565}k_3 + \frac{2197}{4104}k_4 - \frac{1}{5}k_5, \\
\tilde{x}_{i+1} &= x_i + \frac{16}{135}k_1 + \frac{6656}{12825}k_3 + \frac{28561}{56430}k_4 - \frac{9}{50}k_5 + \frac{2}{55}k_6, \\
E &= \frac{1}{h}|\tilde{x}_{i+1} - x_{i+1}| = \frac{1}{h}\left|\frac{1}{360}k_1 - \frac{128}{4275}k_3 - \frac{2197}{75240}k_4 + \frac{1}{50}k_5 + \frac{2}{55}k_6\right|.
\end{aligned}$$

If the error  $E$  is less than the tolerance  $\epsilon$ , the time step is acceptable, then the approximation at the grid point by 4th-order-algorithm is

$$x_{i+1} = x_i + \frac{25}{216}k_1 + \frac{1408}{2565}k_3 + \frac{2197}{4104}k_4 - \frac{1}{5}k_5. \quad (26)$$

If the error  $E$  is greater than tolerance, the error of approximation is unacceptable, a new step size should be determined for further steps. To recalculate a new step size, the scaling factor of the step size,  $\delta$ , is calculate as

$$\delta = 0.84\left(\frac{\epsilon}{E}\right)^{1/4}. \quad (27)$$

When  $\delta \leq 0.1$ , the step size  $h$  is greater than maximum bound, that the approximation is unacceptable. In order to get more accurate approximation, we need to decrease the step size. Replace  $h_{i+1} = 0.1h_i$  provided that the smaller step size satisfies  $h_{i+1} \geq h_{min}$ . Compute new values of  $x_{i+1}$  and  $\tilde{x}_{i+1}$  for this smaller step size.

When  $\delta \geq 4$ , the step size  $h$  is smaller than minimum bound, that the approximation is quite accurate that the step size is more than adequate. In this case, we can increase the step size to accelerate the procedure without losing the accuracy. Increasing  $h$  by four times as long as the larger step size is still smaller than  $h_{max}$ . That is, set  $h_{i+1} = 4h_i$

When  $0.1 < \delta < 4$ , then  $x_{i+1}$  is an acceptable approximation at  $t_{i+1}$ . In this case, step size can be used to calculate the next grid point,  $h_{i+1} = h_i$ . An alternative is to recalculate a new step size with the scaling factor  $\delta$ . Replace  $h_{i+1} = \delta h$ .

Every time when  $h > h_{max}$ , the step size will be reset as  $h = h_{max}$ , so that we keep

the step size in an acceptable range.

Repeat the above steps. If new grid point has  $t \geq b$ , which means the grid point is the end point and the procedure is completed. We stop the process at this point. If the new grid point does not reach the right end of time interval, but the next grid point exceed the interval, that  $t + h > b$ , then set  $h = b - t$ , so that the final point will be set as the end poing of the interval. However, if this  $h$  is smaller than  $h_{min}$ , that minimum  $h$  is exceeded, then the procedure is completed unsuccessfully, but with a small value of  $h_{min}$ , the data collected is sufficient for analysis.

In 4th-order-RK method, the result depends on different prescribed step size, while a large step size results in less accuracy, and a small step size delays the progress. This brings the problem of choosing an appropriate step size. Using the Runge-Kutta-Fehlberg method, the error of the compuation maintains in a local error bound. The adaptive step size solves this problem by automatically resize time steps, that saves time of calculation and guarantees a good approximation.

### 3 Formulation

Consider an unbalanced shaft, mounted on a rigid base, which is suspended on two elastic spring sets vertically and horizontally, allowing the shaft to move translationally in vertical direction  $x$ , and horizontal direction  $y$  (Figure 4). Based on the one dimensional vibration of an unbalanced shaft, Dimentberg et al. [3], the equations of its coupled translational and rotational motion can be written as

$$m\ddot{X} + C\dot{X} + K_x X = -mr \frac{d^2}{dt^2}(\cos \phi) , \quad (28)$$

$$m\ddot{Y} + C\dot{Y} + K_y Y = -mr \frac{d^2}{dt^2}(\sin \phi) , \quad (29)$$

$$I\ddot{\phi} = M(\dot{\phi}, t) + mr(\ddot{X} \sin \phi - \ddot{Y} \cos \phi) + mgr \cos(\phi + \pi/2) . \quad (30)$$

Here  $X(t)$ ,  $Y(t)$  are vertical displacement and horizontal displacement of the shaft's mass center, respectively, and  $\phi(t)$  is the shaft's rotation angle. It is assumed that the unbalanced shaft is torsionally stiff shaft, which means the shaft and motor rotate simul-

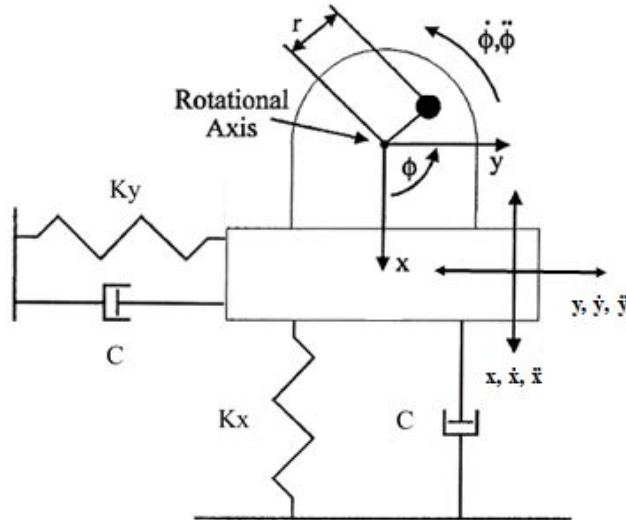


Figure 4: Model of an unbalanced rotating shaft on a support with two-dimensional elastic suspension spring sets.  $x(t)$  and  $y(t)$  are translational displacement in two dimensions,  $\phi$  is the rotation angle of the shaft.

taneously without torsional phase. Although in practical application, the phase generally exists, we are not going to consider this in our problem.  $K_x$  and  $K_y$  are the stiffness of vertical spring set x and horizontal spring set y respectively, while their damping coefficients are assumed to be equal as  $C$ . The unbalanced mass and its eccentricity are denoted as  $m$  and  $r$ , respectively, whereas  $I$  is the shaft's mass moment of inertia such that  $I = m(r_G^2 + r^2)\ddot{\phi}$  where  $r_G$  is the shaft's radius of gyration. The last term on the RHS of the Equation (30) is due to gravity. The influence of gravity for vertical shaft is absent, whereas for a horizontal shaft it is of minor importance at high rotation speeds and high accelerations in both x and y directions.

## Non-Dimensionalization

To simplify our problem, we non-dimensionalize the system. Let

$$x = \frac{X}{r}, \quad y = \frac{Y}{r}, \quad \bar{t} = \sqrt{\frac{K_x}{m}}t = \Omega_x t. \quad (31)$$

where  $\Omega_x$  is the natural frequency of the undamped  $x$ -displacement, which can be derived from Equation (29). Rewrite the equations of system in non-dimensional variables:

$$mr \frac{K_x}{m} \ddot{x} + C \cdot r \sqrt{\frac{K_x}{m}} \dot{x} + r K_x x = -mr \frac{K_x}{m} \frac{d^2}{d\bar{t}^2}(\cos \phi). \quad (32)$$

So that

$$\ddot{x} + \frac{C}{\sqrt{K_x m}} \dot{x} + x = -\frac{d^2}{d\bar{t}^2}(\cos \phi). \quad (33)$$

Substitute damping ratio  $\alpha = \frac{C}{2\sqrt{K_x m}}$  into the equation, we have the non-dimensionalized  $x$ -momentum equation:

$$\ddot{x} + 2\alpha \dot{x} + x = -\frac{d^2}{d\bar{t}^2}(\cos \phi). \quad (34)$$

Similarly, non-dimensionalize the  $y$ -momentum equation with respect to  $\bar{t} = \Omega_x t$ ,

where  $\Omega_x = \sqrt{\frac{K_x}{m}}$ . Let  $\Omega = \frac{\Omega_y}{\Omega_x}$  where  $\Omega_y = \sqrt{\frac{K_y}{m}}$ , we get:

$$\ddot{y} + 2\alpha\dot{y} + \Omega^2 y = -\frac{d^2}{dt^2}(\sin \phi) . \quad (35)$$

Rewrite the angular momentum equation in  $\bar{t}$ :

$$\frac{K_x}{m}\ddot{\phi} - \left( r\frac{K_x}{m}\ddot{x}\sin\phi - r\frac{K_x}{m}\ddot{y}\cos\phi \right) = \frac{M}{m(r_G^2 + r^2)} . \quad (36)$$

Let  $\epsilon = \frac{r}{r_G}$  and  $\bar{M} = \frac{M}{K_x(r_G^2 + r^2)}$ , Equation (36) becomes:

$$\bar{M} = \ddot{\phi} - \frac{\epsilon^2}{1 + \epsilon^2} (\ddot{x}\sin\phi - \ddot{y}\cos\phi) . \quad (37)$$

From the equation of  $\bar{M}$ , we can see that  $\bar{M}$  is on the order of  $\epsilon^2$ . In next section, we apply analytical methods to approximate the values of  $\bar{M}$ .

## 4 Steady-state Response

The general function of simple harmonic motion:  $m\ddot{x} + c\dot{x} + kx = F_0 \sin(\omega t)$  has solution of displacement  $x(t) = X \sin(\omega_n t - \theta_1) + A \exp(-\epsilon \omega_n t) \sin(\omega_d t + \theta_2)$ , where  $X$  and  $A$  are constant amplitudes,  $\phi$  and  $\phi_1$  are phase angles,  $\omega$  is the force frequency,  $\omega_n$  is the natural frequency, and  $\omega_d$  is the damped natural frequency. The first part of the equation denotes the steady-state response and the second part corresponds to the transient response. In the analytical analysis, we only apply the KB-averaging method to find the steady-state response. The transient response is found by numerical simulation in next section.

In our problem, we use different notations such that  $\phi$  is the rotation angle of the shaft, and  $\nu = \dot{\phi}$  is the rotational velocity, which for steady-state case  $\nu$  is a constant. The solution of our problem is:

$$x(\bar{t}) = X_s \sin(\nu \bar{t}) + X_c \cos(\nu \bar{t}) , \quad (38)$$

$$y(\bar{t}) = Y_s \sin(\nu \bar{t}) + Y_c \cos(\nu \bar{t}) . \quad (39)$$

Since the steady-state rotational velocity  $\nu = \text{constant}$ , we have  $\ddot{\phi} = \dot{\nu} = 0$ . Therefore the RHS of the equations of translational vibrations can be expanded with  $\ddot{\phi} = 0$ , so that the equations of system are:

$$\ddot{x} + 2\alpha\dot{x} + x = \nu^2 \cos(\nu \bar{t}) , \quad (40)$$

$$\ddot{y} + 2\alpha\dot{y} + \Omega_y^2 y = \nu^2 \sin(\nu \bar{t}) , \quad (41)$$

$$\bar{M} = \frac{\epsilon^2}{1 + \epsilon^2} [-\ddot{x} \sin(\nu \bar{t}) + \ddot{y} \cos(\nu \bar{t})] . \quad (42)$$

Substitute the solution of  $x(\bar{t})$ , (38), into Equation (40):

$$(1 - \nu^2)(X_c \cos(\nu \bar{t}) + X_s \sin(\nu \bar{t})) + 2\alpha(-\nu X_c \sin(\nu \bar{t}) + \nu X_s \cos(\nu \bar{t})) = \epsilon \nu^2 \cos(\nu \bar{t}) . \quad (43)$$

By equating the  $\sin(\nu\bar{t})$  terms and  $\cos(\nu\bar{t})$  terms, we solve for  $X_s$  and  $X_c$ :

$$X_s = \frac{2\alpha\nu^3}{\Gamma_x}, \quad (44)$$

$$X_c = \frac{\nu^2(1 - \nu^2)}{\Gamma_x}, \quad (45)$$

where  $\Gamma_x = (1 - \nu^2)^2 + (2\alpha\nu)^2$ .

Similarly, substitute the solution of  $y(\bar{t})$ , (39), into Equation (41):

$$(\Omega^2 - \nu^2)(Y_c \cos(\nu\bar{t}) + Y_s \sin(\nu\bar{t})) + 2\alpha(-\nu Y_c \sin(\nu\bar{t}) + \nu Y_s \cos(\nu\bar{t})) = \epsilon\nu^2 \sin(\nu\bar{t}), \quad (46)$$

and equate  $\sin(\nu\bar{t})$  terms and  $\cos(\nu\bar{t})$  of two sides, we can find:

$$Y_s = \frac{\nu^2(\Omega^2 - \nu^2)}{\Gamma_y}, \quad (47)$$

$$Y_c = -\frac{2\alpha\nu^3}{\Gamma_y}, \quad (48)$$

where  $\Gamma_y = (\Omega^2 - \nu^2)^2 + (2\alpha\nu)^2$ .

Since  $\bar{M}$  is in the order of  $O(\epsilon^2)$ , as introduced in previous section, we can apply KB-averaging method to find this as a function of  $\nu$ .

$$\begin{aligned} \bar{M}(\nu) &= \frac{\epsilon^2}{1 + \epsilon^2} \left( \frac{\nu}{2\pi} \right) \int_0^{2\pi/\nu} (X_c \sin(\nu t) \cos(\nu t) + X_s \sin(\nu t)^2 - Y_s \sin(\nu t) \cos(\nu t) - Y_c \cos(\nu t)^2) dt \\ &= \frac{\epsilon^2}{1 + \epsilon^2} \left( \frac{\nu}{2\pi} \right) \int_0^{2\pi/\nu} (X_s \sin(\nu t)^2 - Y_c \cos(\nu t)^2) dt \\ &= \frac{\epsilon^2}{2(1 + \epsilon^2)} (X_s - Y_c), \end{aligned} \quad (49)$$

since the average of  $X_c \sin(\nu t) \cos(\nu t)$  and  $Y_s \sin(\nu t) \cos(\nu t)$  are zero.

Substitute  $X_s$  and  $Y_c$  into the equation of  $\bar{M}$ :

$$\bar{M}_{ss} = \frac{\alpha\nu^3\epsilon^2}{1 + \epsilon^2} \left( \frac{1}{\Gamma_x} + \frac{1}{\Gamma_y} \right). \quad (50)$$

The following figure demonstrates the curve of the steady-state threshold torque  $\bar{M}_{ss}$ , such that starting with a driving torque  $M$ , the system will reach a point on the curve that corresponds to its steady-state. There exist two peaks of the curve, which locate at  $\nu = 1$  and  $\nu = \Omega$ , and correspond to x-resonance and y-resonance. The stability of the steady-state curve is analyzed later.

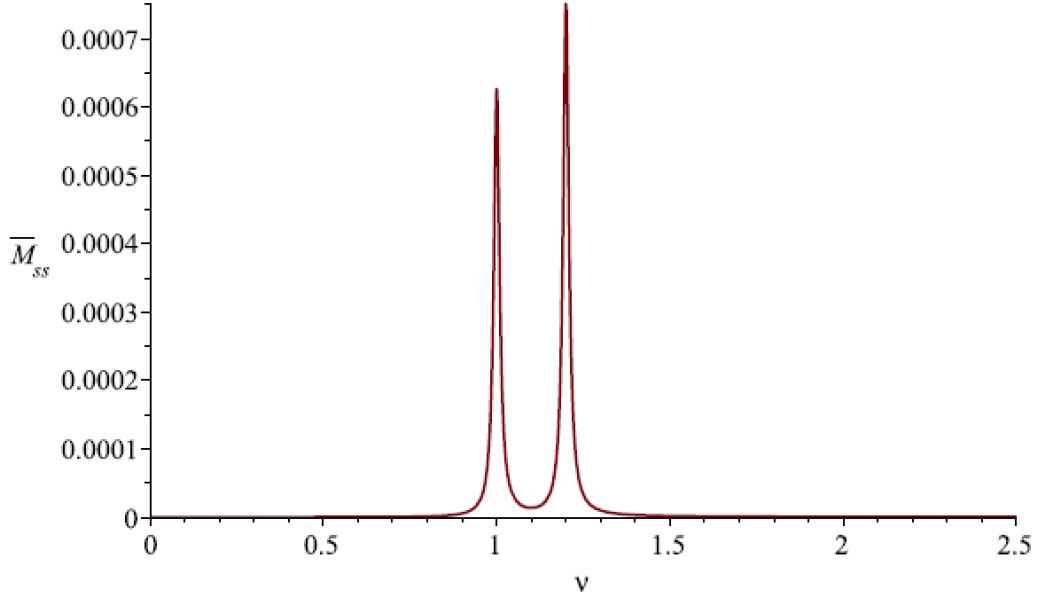


Figure 5: Steady-state curve of threshold torque  $\bar{M}_{ss}$  vs. angular velocity  $\nu$ , with  $\alpha = 0.01$ ,  $\epsilon = 0.005$  and  $\Omega = 1.2$

Consider the values of steady-state torque  $\bar{M}_{ss}$  of the two peaks:  $\nu = 1$  and  $\nu = \Omega$ , they are functions depending on  $\Omega$ . From the function of  $\bar{M}_{ss}$ , Eq (50), when  $\nu$  reaches 1, the function of steady-state torque is:

$$(\bar{M}_{ss})_1 = \frac{\alpha\epsilon^2}{1 + \epsilon^2} \left( \frac{1}{4\alpha^2} + \frac{1}{(\Omega^2 - 1)^2 + 4\alpha^2} \right). \quad (51)$$

The plot of  $(\bar{M}_{ss})_1$ , with  $\alpha = 0.01$  and  $\epsilon = 0.005$  is demonstrated in Figure 6. As we consider the cases between two extreme cases: axisymmetric case and one-dimensional case, we only care about the range of  $\Omega$  that is  $1 \leq \Omega \leq \infty$ . When  $\Omega = 1$ , the system is axisymmetric, such that the horizontal and vertical spring sets have the same spring

stiffness. In this case, the value of  $(\bar{M}_{ss})_1$  is around 0.00125, which is the first peak value of  $\bar{M}_{ss}$  at  $\nu = 1$ . For the one-dimensional case, which can be denoted as  $\Omega = \infty$ , the second peak value of  $\bar{M}_{ss}$  at  $\nu = \Omega$  is around 0.000625, which is one half of the steady-state torque value in axisymmetric case. And as indicated in the figure, the  $(\bar{M}_{ss})_1$  curve decreases from the maximum value at  $\Omega = 1$ , and is asymptotic to the value of one-dimensional case, 0.000625.

Now consider the second peak at  $\nu = \Omega$ , the steady-state torque is:

$$(\bar{M}_{ss})_2 = \frac{\alpha\epsilon^2\Omega^3}{1 + \epsilon^2} \left( \frac{1}{(1 - \Omega^2)^2 + 4\alpha^2\Omega^2} + \frac{1}{4\alpha^2\Omega^2} \right). \quad (52)$$

Different from the  $(\bar{M}_{ss})_1$  curve, the values at the peak  $\nu = \Omega$  decreases from the maximum value 0.00125 at axisymmetric case  $\Omega = 1$ , reaches its minimum value 0.000681 at  $\Omega = 1.058$ , and increases again to infinity. Since the minimum value of  $(\bar{M}_{ss})_2$  is greater than all the values in  $(\bar{M}_{ss})_1$ , the steady-state torque  $\bar{M}_{ss}$  at the second peak  $\nu = \Omega$  is always above the steady-state torque at the first peak  $\nu = 1$ . This is also inferred from the  $\bar{M}_{ss}$  function, Eq (50).

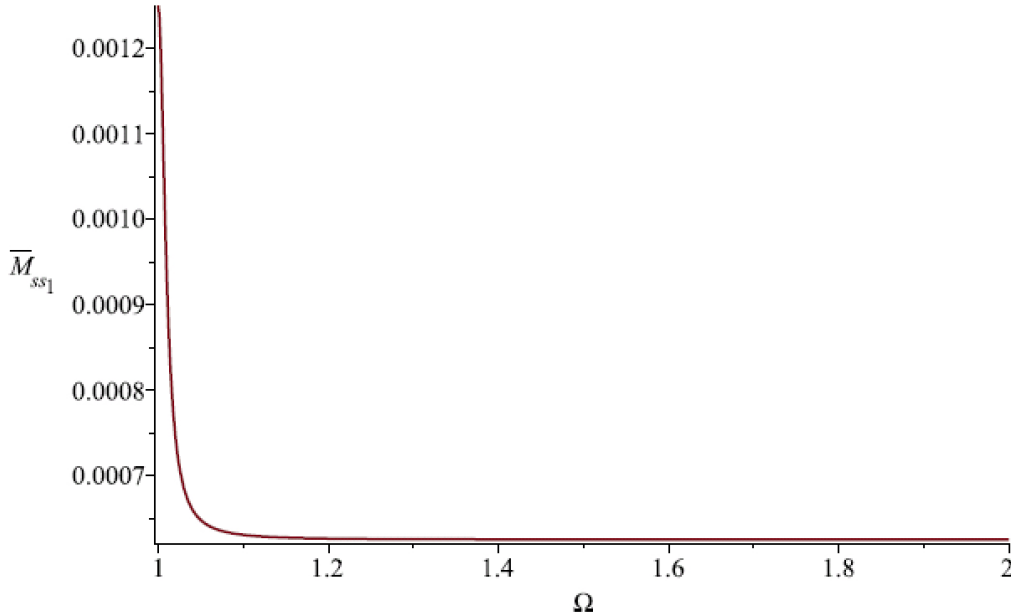


Figure 6: Threshold steady-state torque values at  $\nu = 1$ ,  $(\bar{M}_{ss})_1$  vs. angular velocity  $\nu$ , with  $\alpha = 0.01$ , and  $\epsilon = 0.005$

With this property of curve  $(\bar{M}_{ss})_2$ , we introduce a passage technique for axisymmetric vibrating system, by slightly increasing the spring stiffness. Suppose the vibrating system is axisymmetric, such that the x-axis spring stiffness equals the y-axis spring stiffness, the technically required torque for passage is 0.00125, as found above. This means at least 0.00125 of torque is needed for passage over resonance. If the y-axis spring stiffness is slightly raised from 1 to 1.058, then the minimum torque required for passage in x-displacement is 0.000625, and the minimum torque required for y-displacement passage is 0.000681. Hence with x-axis spring stiffness being unity, and y-axis spring stiffness being 1.058, the torque required for passage in both x-displacement and y-displacement is 0.000681. Thus, for a axisymmetric vibration system with input torque between 0.000681 and 0.00125, which is captured at resonance initially, a slightly increase of  $y$ -axis spring stiffness by 0.058 will achieve passage over resonance at  $\nu = \Omega$ .

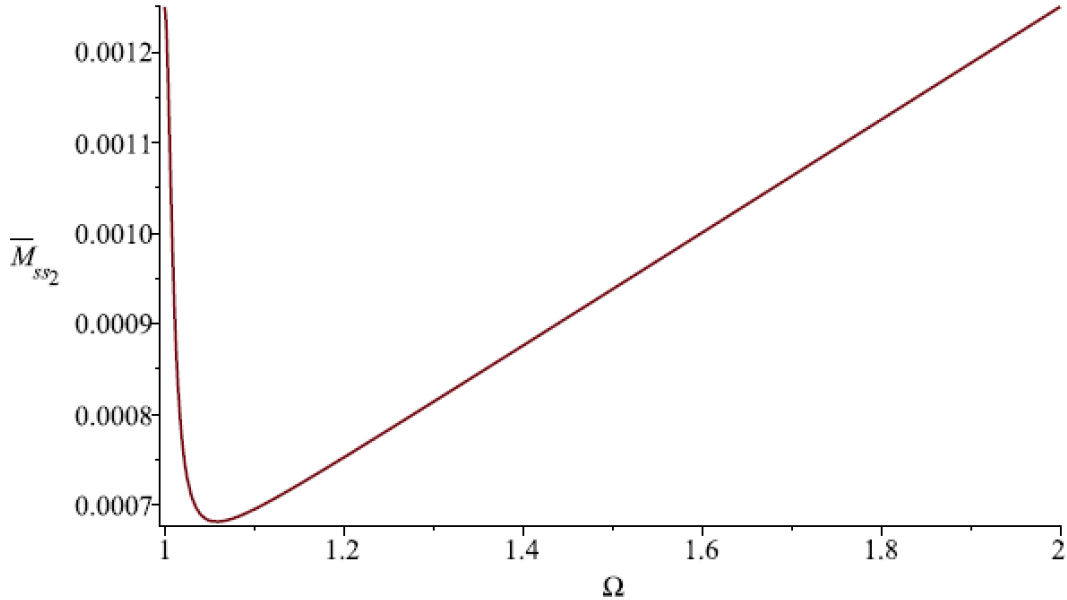


Figure 7: Threshold steady-state torque values at  $\nu = \Omega$ ,  $(\bar{M}_{ss})_2$  vs. angular velocity  $\nu$ , with  $\alpha = 0.01$ ,  $\epsilon = 0.005$ , and  $\Omega = 1.2$

## 5 Transient Response

In previous section, we consider the steady-state response, while before the vibration reaches steady state, we also need to consider the transient case. The figure of steady-state torque demonstrates the the final angular velocity  $\dot{\phi}$  that the shaft will reach, with some given initial conditions. In this section, we apply perturbation expansion, as well as KB-averaging, to look for the general solution of displacement equations. Since from the equation of steady-state torque, Eq (50),  $\bar{M}_{ss}$  is of order  $\epsilon^2$ , the terms of order  $\epsilon^2$  in the perturbation expansion of angular momentum equation corresponds to the steady-state torque.

Steady-state response has stability criteria, such that vibration approaches stable steady state, but departs from unstable steady state. Hence with the analysis of transient response, we are able to determine the vibrations with initial conditions that is not located on the steady-state torque curve.

Starting with the analysis of transient response, the equations of system are:

$$\ddot{x} + 2\alpha\dot{x} + x = \dot{\phi}^2 \cos \phi + \ddot{\phi} \sin \phi , \quad (53)$$

$$\ddot{y} + 2\alpha\dot{y} + \Omega^2 y = \dot{\phi}^2 \sin \phi - \ddot{\phi} \cos \phi , \quad (54)$$

$$\bar{M} = \epsilon^2 \bar{\phi}'' + \frac{\epsilon^2}{1 + \epsilon^2} (\ddot{y} \cos \phi - \ddot{x} \sin \phi) . \quad (55)$$

Consider  $\phi = \nu t + \bar{\phi}(\tau)$ , where  $\bar{\phi}(\tau)$  denotes the perturbation added to the constantly increasing rotation angle  $\phi$ . A new time scale  $\tau$  is of the order of  $\epsilon$ , such that  $\tau = \epsilon t$ . With the new time scale  $\tau$ , let

$$x = x_s(\tau) \sin \nu t + x_c(\tau) \cos \nu t , \quad (56)$$

$$y = y_s(\tau) \sin \nu t + y_c(\tau) \cos \nu t . \quad (57)$$

Then

$$\dot{x} = \nu x_s \cos \nu t - \nu x_c \sin \nu t + \epsilon(x'_s \sin \nu t + x'_c \cos \nu t) , \quad (58)$$

$$\ddot{x} = -\nu^2 x + 2\epsilon\nu(x'_s \cos \nu t - x'_c \sin \nu t) + \epsilon^2(x''_s \sin \nu t + x''_c \cos \nu t) \quad (59)$$

where  $x'_s$  denotes derivative of  $x_s$  with respect to  $\tau$ , similarly for  $x'_c$ ,  $x''_s$  and  $x''_c$ .

Substitute these expressions into the  $x$ -momentum equation (53) and factorize out  $\sin \nu t$  and  $\cos \nu t$  for the left hand side:

$$\begin{aligned} & [(1 - \nu^2)x_s - 2\epsilon\nu x'_c + \epsilon^2 x''_s - 2\alpha\nu x_c + 2\alpha\epsilon x'_s] \sin \nu t \\ & + [(1 - \nu^2)x_c + 2\epsilon\nu x'_s + \epsilon^2 x''_c + 2\alpha\nu x_s + 2\alpha\epsilon x'_c] \cos \nu t \\ & = (\nu + \epsilon\bar{\phi}')^2 (\cos \nu t \cos \bar{\phi} - \sin \nu t \sin \bar{\phi}) + \epsilon^2 \bar{\phi}'' (\sin \nu t \cos \bar{\phi} + \cos \nu t \sin \bar{\phi}) . \end{aligned} \quad (60)$$

For the  $\sin \nu t$  terms and  $\cos \nu t$  terms, there are two equations:

$$(1 - \nu^2)x_s - 2\alpha\nu x_c + 2\epsilon(\alpha x'_s - \nu x'_c) + \epsilon^2 x''_s = -(\nu + \epsilon\bar{\phi}')^2 \sin \bar{\phi} + \epsilon^2 \bar{\phi}'' \cos \bar{\phi} , \quad (61)$$

$$(1 - \nu^2)x_c - 2\alpha\nu x_s + 2\epsilon(\alpha x'_c + \nu x'_s) + \epsilon^2 x''_c = (\nu + \epsilon\bar{\phi}')^2 \cos \bar{\phi} + \epsilon^2 \bar{\phi}'' \sin \bar{\phi} . \quad (62)$$

Expand  $x_s$  and  $x_c$  in a regular perturbation expansion:

$$\begin{pmatrix} x_s \\ x_c \end{pmatrix} = \begin{pmatrix} x_{s0} \\ x_{c0} \end{pmatrix} + \epsilon \begin{pmatrix} x_{s1} \\ x_{c1} \end{pmatrix} + \dots . \quad (63)$$

At leading order, we find:

$$\begin{pmatrix} 1 - \nu^2 & -2\alpha\nu \\ 2\alpha\nu & 1 - \nu^2 \end{pmatrix} \begin{pmatrix} x_{s0} \\ x_{c0} \end{pmatrix} = \nu^2 \begin{pmatrix} -\sin \bar{\phi} \\ \cos \bar{\phi} \end{pmatrix} \quad (64)$$

Solve this system (64) to find  $x_{s_0}$  and  $x_{c_0}$ :

$$x_{s_0} = \frac{\nu^2}{\Gamma_x} [2\alpha\nu \cos \bar{\phi} - (1 - \nu^2) \sin \bar{\phi}] , \quad (65)$$

$$x_{c_0} = \frac{\nu^2}{\Gamma_x} [(1 - \nu^2) \cos \bar{\phi} + 2\alpha\nu \sin \bar{\phi}] , \quad (66)$$

where  $\Gamma_x = (1 - \nu^2)^2 + (2\alpha\nu)^2$ .

Note that,

$$x'_{c_0} = \bar{\phi}' x_{s_0} , \quad (67)$$

$$x'_{s_0} = -\bar{\phi}' x_{c_0} . \quad (68)$$

At  $O(\epsilon)$ , we find that

$$\begin{pmatrix} 1 - \nu^2 & -2\alpha\nu \\ 2\alpha\nu & 1 - \nu^2 \end{pmatrix} \begin{pmatrix} x_{s_1} \\ x_{c_1} \end{pmatrix} = 2\nu\bar{\phi}' \begin{pmatrix} -\sin \bar{\phi} \\ \cos \bar{\phi} \end{pmatrix} + 2\bar{\phi}' \begin{pmatrix} \nu & \alpha \\ -\alpha & \nu \end{pmatrix} \begin{pmatrix} x_{s_0} \\ x_{c_0} \end{pmatrix} , \quad (69)$$

$$\begin{pmatrix} x_{s_1} \\ x_{c_1} \end{pmatrix} = 2\bar{\phi}' \begin{pmatrix} B_x x_{s_0} + A_x x_{c_0} \\ -A_x x_{s_0} + B_x x_{c_0} \end{pmatrix} , \quad (70)$$

where

$$A_x = \frac{\alpha(1 + \nu^2)}{\Gamma_x} , \quad (71)$$

$$B_x = \frac{1}{\nu} + \frac{\nu(1 - \nu^2) - 2\alpha^2\nu}{\Gamma_x} . \quad (72)$$

Now consider the  $y$ -momentum equation (54). Let  $y = y_s(\tau) \sin \nu t + y_c(\tau) \cos \nu t$ , find the first and second derivative of  $y$  with respect to  $t$ :

$$\dot{y} = \nu y_s \cos \nu t - \nu y_c \sin \nu t + \epsilon(y'_s \sin \nu t + y'_c \cos \nu t) , \quad (73)$$

$$\ddot{y} = -\nu y^2 + 2\epsilon\nu(y'_s \cos \nu t - y'_c \sin \nu t) + \epsilon^2(y''_s \sin \nu t + y''_c \cos \nu t) . \quad (74)$$

Substitute Eq (73) and (74) into equation (54). Separate the  $\sin \nu t$  terms and  $\cos \nu t$  terms:

$$(\Omega^2 - \nu^2)y_s - 2\alpha\nu y_c + 2\epsilon(\alpha y'_s - \nu y'_c) + \epsilon^2 y''_s = (\nu + \epsilon\bar{\phi}')^2 \cos \bar{\phi} + \epsilon^2 \bar{\phi}'' \sin \bar{\phi} , \quad (75)$$

$$(\Omega^2 - \nu^2)y_c + 2\alpha\nu y_s + 2\epsilon(\alpha y'_c + \nu y'_s) + \epsilon^2 y''_c = (\nu + \epsilon\bar{\phi}')^2 \sin \bar{\phi} - \epsilon^2 \bar{\phi}'' \cos \bar{\phi} . \quad (76)$$

Expand  $y_s$  and  $y_c$  in a regular perturbation expansion:

$$\begin{pmatrix} y_s \\ y_c \end{pmatrix} = \begin{pmatrix} y_{s0} \\ y_{c0} \end{pmatrix} + \epsilon \begin{pmatrix} y_{s1} \\ y_{c1} \end{pmatrix} + \dots , \quad (77)$$

then at  $O(1)$ , we find that:

$$\begin{pmatrix} \Omega^2 - \nu^2 & -2\alpha\nu \\ 2\alpha\nu & \Omega^2 - \nu^2 \end{pmatrix} \begin{pmatrix} y_{s0} \\ y_{c0} \end{pmatrix} = \nu^2 \begin{pmatrix} \cos \bar{\phi} \\ \sin \bar{\phi} \end{pmatrix} , \quad (78)$$

which has the solution

$$y_{s0} = \frac{\nu^2}{\Gamma_y} [(\Omega^2 - \nu^2) \cos \bar{\phi} + 2\alpha\nu \sin \bar{\phi}] , \quad (79)$$

$$y_{c0} = \frac{\nu^2}{\Gamma_y} [-2\alpha\nu \cos \bar{\phi} + (\Omega^2 - \nu^2) \sin \bar{\phi}] , \quad (80)$$

where  $\Gamma_y = (\Omega^2 - \nu^2)^2 + (2\alpha\nu)^2$ .

Similar to the  $x$ -component case,

$$y'_{s0} = -\bar{\phi}' y_{c0} , \quad (81)$$

$$y'_{c0} = \bar{\phi}' y_{s0} . \quad (82)$$

Substitute into the terms of order  $\epsilon$  to find  $y_{s1}$  and  $y_{c1}$ :

$$\begin{pmatrix} y_{s1} \\ y_{c1} \end{pmatrix} = 2\bar{\phi}' \begin{pmatrix} B_y y_{s0} + A_y y_{c0} \\ -A_y y_{s0} + B_y y_{c0} \end{pmatrix} , \quad (83)$$

where

$$A_y = \frac{\alpha(\Omega^2 + \nu^2)}{\Gamma_y}, \quad (84)$$

$$B_y = \frac{1}{\nu} + \frac{\nu(\Omega^2 - \nu^2) - 2\alpha^2\nu}{\Gamma_y}. \quad (85)$$

Substitute  $x_s$ ,  $x_c$  and  $y_s$ ,  $y_c$  into the momentum equation (55), and apply KB-averaging:

$$\begin{aligned} \bar{M} = \epsilon^2 \bar{\phi}'' + \frac{\epsilon^2}{1 + \epsilon^2} & \left[ \frac{\nu^2}{2} (y_s \sin \bar{\phi} - y_c \cos \bar{\phi}) + \epsilon \nu (y'_s \cos \bar{\phi} + y'_c \sin \bar{\phi}) + \frac{\epsilon^2}{2} (-y''_s \sin \bar{\phi} + y''_c \cos \bar{\phi}) \right. \\ & \left. + \frac{\nu^2}{2} (x_s \cos \bar{\phi} + x_c \sin \bar{\phi}) - \epsilon \nu (x'_s \sin \bar{\phi} - x'_c \cos \bar{\phi}) - \frac{\epsilon^2}{2} (x''_s \cos \bar{\phi} + x''_c \sin \bar{\phi}) \right]. \end{aligned} \quad (86)$$

Substitute the  $x_s$  and  $x_c$  with perturbation term, as well as  $y_s$  and  $y_c$  into the equation (86), the terms of order  $\epsilon^2$  can be simplified as

$$\alpha \nu^3 \left( \frac{1}{\Gamma_x} + \frac{1}{\Gamma_y} \right) = \bar{M}_{ss} \left( \frac{1 + \epsilon^2}{\epsilon^2} \right),$$

which corresponds to the simple harmonic case.

## Stability of steady-state response

By considering the terms of order  $\epsilon^2$ , we derived the steady-state threshold torque  $\bar{M}_{ss}$ . Continue for the terms of order  $\epsilon^3$ , we analyze the transient response.

At order  $\epsilon^3$ , we have:

$$\begin{aligned} \nu (y'_{s_0} \cos \bar{\phi} + y'_{c_0} \sin \bar{\phi}) + \frac{\nu^2}{2} (y_{s_1} \sin \bar{\phi} - y_{c_1} \cos \bar{\phi}) \\ - \nu (x'_{s_0} \sin \bar{\phi} - x'_{c_0} \cos \bar{\phi}) + \frac{\nu^2}{2} (x_{s_1} \cos \bar{\phi} + x_{c_1} \sin \bar{\phi}) \end{aligned}$$

$$\begin{aligned}
&= \nu(-\bar{\phi}'y_{c_0} \cos \bar{\phi} + \bar{\phi}'y_{s_0} \sin \bar{\phi}) + \nu^2\bar{\phi}'[(B_y y_{s_0} + A_y y_{c_0}) \sin \bar{\phi} \\
&\hspace{20em} + (A_y y_{s_0} - B_y y_{c_0}) \cos \bar{\phi}] \\
&\quad + \nu(\bar{\phi}'x_{c_0} \sin \bar{\phi} + \bar{\phi}'x_{s_0} \cos \bar{\phi}) + \nu^2\bar{\phi}'[(B_x x_{s_0} + A_x x_{c_0}) \cos \bar{\phi} \\
&\hspace{20em} (-A_x x_{s_0} + B_x x_{c_0}) \sin \bar{\phi}] \\
&= \bar{\phi}'\{-\nu y_{c_0} \cos \bar{\phi} + \nu y_{s_0} \sin \bar{\phi} + \nu^2[(B_y y_{s_0} + A_y y_{c_0}) \sin \bar{\phi}] + (A_y y_{s_0} - B_y y_{c_0}) \cos \bar{\phi}\} \\
&\quad + \nu x_{c_0} \sin \bar{\phi} + \nu x_{s_0} \cos \bar{\phi} + \nu^2[(B_x x_{s_0} + A_x x_{c_0}) \cos \bar{\phi}(-A_x x_{s_0} + B_x x_{c_0}) \sin \bar{\phi}]
\end{aligned} \tag{87}$$

Then with the perturbation expansion of the momentum equation Eq.(55), we have

$$\bar{M} = \epsilon^2 \bar{\phi}'' + \frac{\epsilon^2}{1 + \epsilon^2} \left[ \alpha \nu^3 \left( \frac{1}{\Gamma_x} + \frac{1}{\Gamma_y} \right) + \epsilon \beta \bar{\phi}' + O(\epsilon^2) \right]. \tag{88}$$

where

$$\beta = \frac{\nu^4}{\Gamma_x} [2\alpha + 2\alpha\nu B_x + A_x(1 - \nu^2)] + \frac{\nu^4}{\Gamma_y} [2\alpha + 2\alpha\nu B_y + A_y(\Omega^2 - \nu^2)]. \tag{89}$$

When  $\bar{M} = \bar{M}_{ss}$ , Eq (88) defines a stability problem for the phase of the form, so that

$$\bar{\phi}'' + \epsilon \beta \bar{\phi}' = 0. \tag{90}$$

Thus, when  $\beta > 0$ , the angular velocity  $\bar{\phi}' = e^{-\beta\tau}$  decays exponentially, and the system is stable. If  $\beta < 0$ , then the angular velocity  $\bar{\phi}'$  grows exponentially, which means unstable.

$$\beta = \frac{\nu^4}{\Gamma_x} [2\alpha + 2\alpha\nu B_x + A_x(1 - \nu^2)] + \frac{\nu^4}{\Gamma_y} [2\alpha + 2\alpha\nu B_y + A_y(\Omega^2 - \nu^2)]. \tag{91}$$

The following are the figures of  $\beta$  vs. angular velocity  $\nu$  with different values of  $\Omega$ . With  $1 \leq \Omega < 1.05$ , as indicated in figure 8 a) and b),  $\beta$  is positive when  $\nu \leq 1$  but

negative when  $\nu > 1$ , and it is asymptotic with respect to 0. However, when  $\Omega \geq 1.5$ ,  $\beta$  splits in three parts.  $\beta$  changes its sign from positive to negative when  $\nu \approx 1$ , and its sign changes from positive to negative again when  $\nu \approx \Omega$ . Compare figure 8 d) with figure 9, we can find when  $\alpha = 0.01$ ,  $\Omega = 1.2$ ,  $\beta$  is positive when the slope of the  $\bar{M}_{ss}$  curve is positive, which is denoted as the blue curves, and  $\beta$  is negative when the slope of the  $\bar{M}_{ss}$  is negative, which is denoted as the red dashed curves.

When the vibration approaches the stable steady state, which are the blue curves in Figure 9, the corresponding rotation speed  $\nu$  denotes the final rotating speed that the shaft gets. This means after the transient state, the shaft reaches its steady state, with rotating speed at a constant value. This corresponds to the capture at resonance, hence

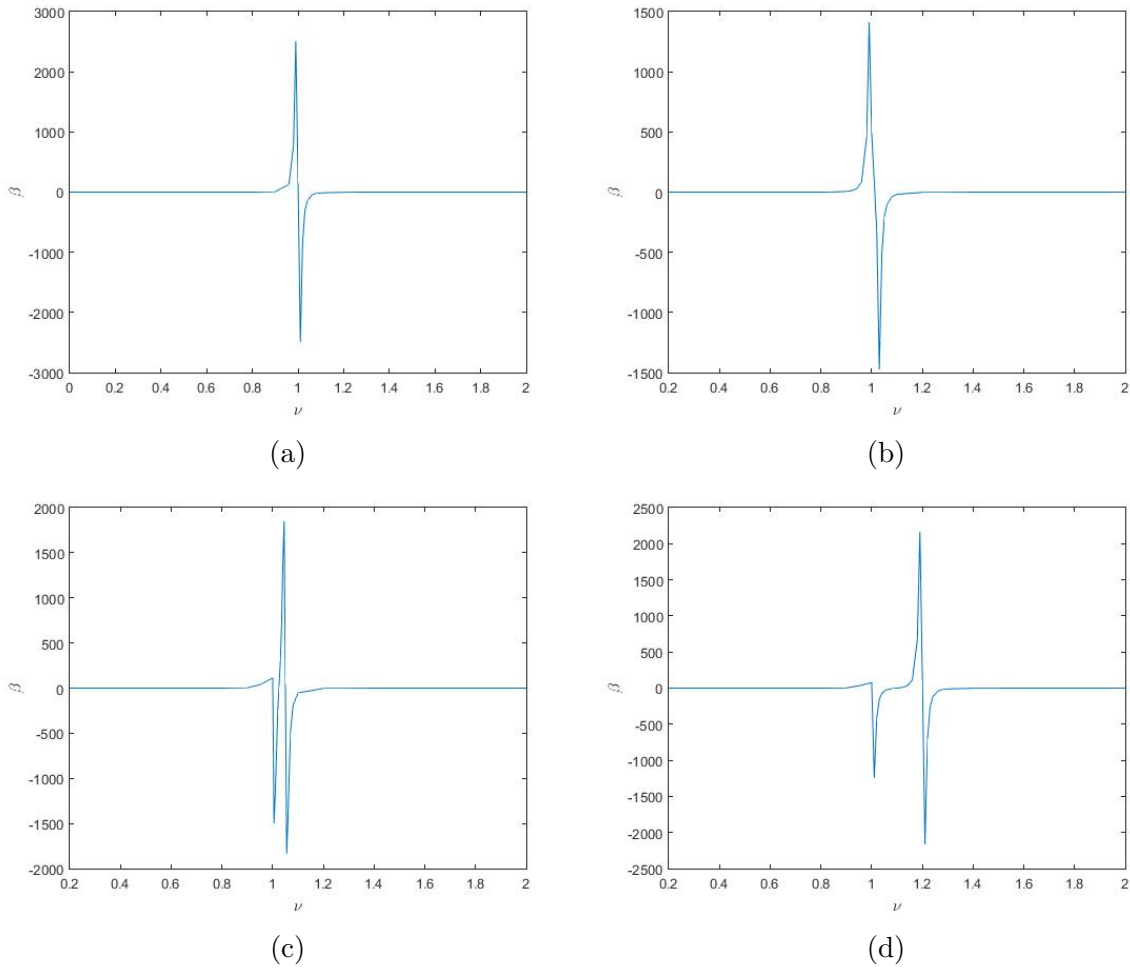


Figure 8: Stability indicator  $\beta$  vs. angular velocity  $\nu$ , with  $\alpha = 0.01$ , and a)  $\Omega = 1$ , b)  $\Omega = 1.02$ , c)  $\Omega = 1.05$ , d)  $\Omega = 1.2$

the rotation of shaft sticks at a constant value, and the vibration amplitude maintains at the large resonant amplitude. With given initial rotation speed and the function of motor torque, we are able to determine the technical capture/passage of shaft based on this figure, as well as the final rotation speed that the shaft reaches.

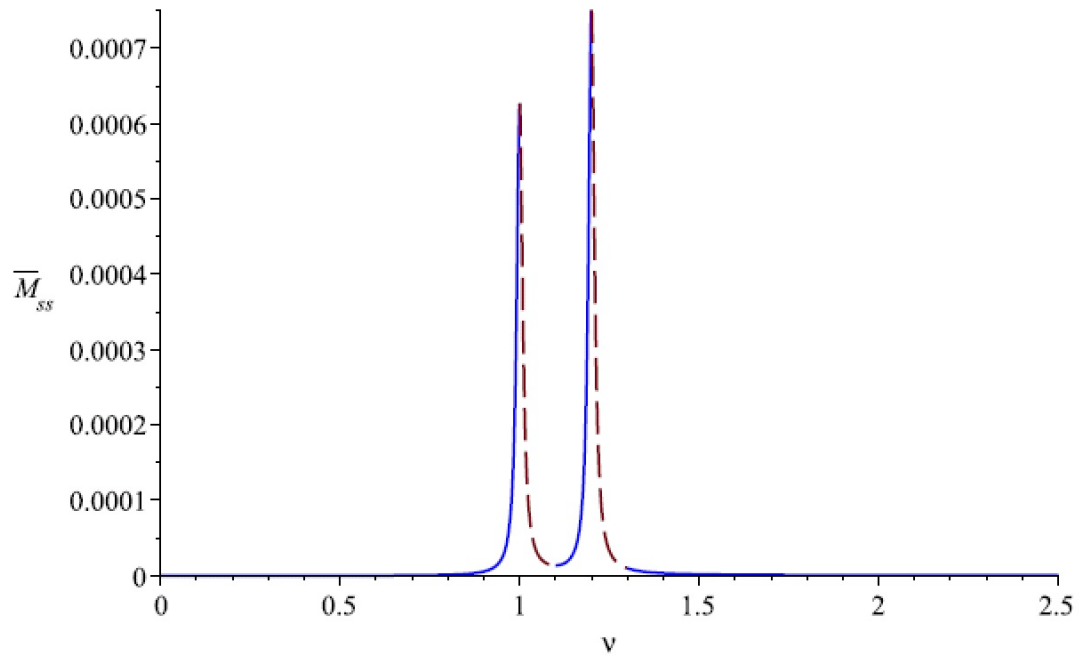


Figure 9: Steady-state stability curve of threshold torque  $\bar{M}_{ss}$  vs. angular velocity  $\nu$ , with  $\alpha = 0.01$ ,  $\epsilon = 0.001$  and  $\Omega = 1.2$ . Blue curve indicates stable steady states, red dashed curve indicates unstable steady states.

## 6 Numerical Simulation

From the previous analysis, we derived the function of steady-state threshold torque  $\bar{M}_{ss}(\nu)$ , and considered transient reponse by using perturbation expansion and KB-averaging. In this chapter, we use numerical simulation to validate the steady-state torque function  $\bar{M}_{ss}(\nu)$ , which leads to a passage technique, and prove the stability criteria of steady-state.

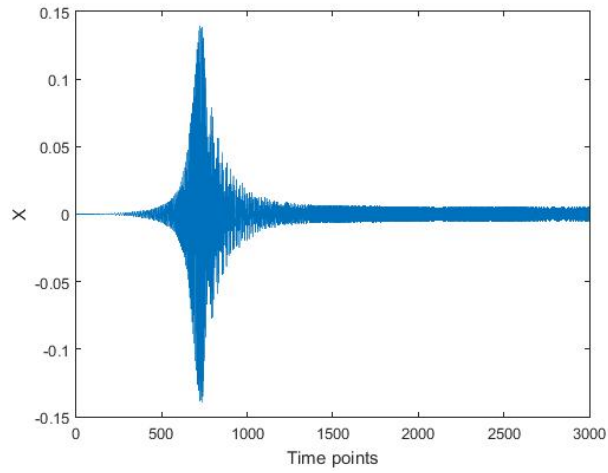
### Passage/Capture

As described in previous sections, the motor torque determines whether the passage or capture will occur in a vibration. Since the power input of the motor keeps constant, there is a tradeoff between the angular velocity of rotation and the motor torque. Thus by increasing the angular velocity of the motor and the shaft, the function of motor torque decays with respect to  $\nu$ . This decaying function of motor torque  $\bar{M}$  depending on angular velocity  $\nu$  is determined by the properties of different kinds of motor. In order to simplify the problem, we assume that the motor torque remains constant no matter how fast the shaft rotates, i.e.  $\bar{M}(\nu) = \bar{M}_0$ . We would like to find  $\bar{M}_0$  as the minimum torque required for passage, and the values of  $\bar{M}_0$  at different values of  $\nu$  correspond to the steady-state response threshold torque  $\bar{M}_{ss}$  by the numerical approach.

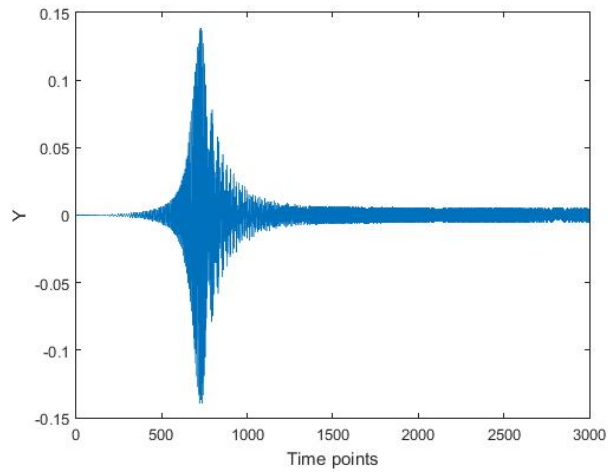
To look for  $\bar{M}_0$ , we need to determine the two cases: passage and capture. As introduced in previous section, passage indicates amplitude of vibration passes over the resonant amplitude and returns to a smaller constant value, while the angular velocity increases throughout the whole process, although some slow down of angular acceleration is possible when passing over the resonance. An example of passage is demonstrated in Figure 10. Capture indicates the case when the vibration reaches its resonance, and the amplitude is captured at the resonant amplitude, which has a high value. The angular velocity of vibration captured at resonance will also be captured at a constant value,

so that the power input is used to vibrate the system instead of increasing the angular velocity. The corresponding figure of capture case is Figure 11.

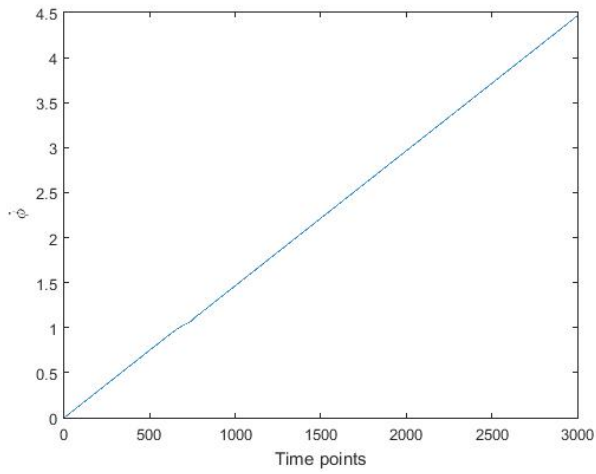
In Dimentberg et al. [3], it introduced the case of “slow passage”, which is passage with an obvious slowdown of angular acceleration. In this case, during the time passing over the resonance, the angular velocity nearly remains constant, which shown in the graph as the gradient of  $\dot{\phi}(t)$  is oscillating about 0. An example of “slow passage” is demonstrated in Figure 12, during the passage over x-resonance and y-resonance, the angular velocity remains at a constant value for a while, and it increases again when the resonance is passed over. “Slow passage” indicates an eventually passage over resonance after an amount of time with rotation velocity remains nearly constant, but a boundary needs to be set in order to differentiate passage and capture. In our research, we only consider passage as increasing angular velocity without gradient being less than 0, which means the “slow passage” will not be considered as passage.



(a)

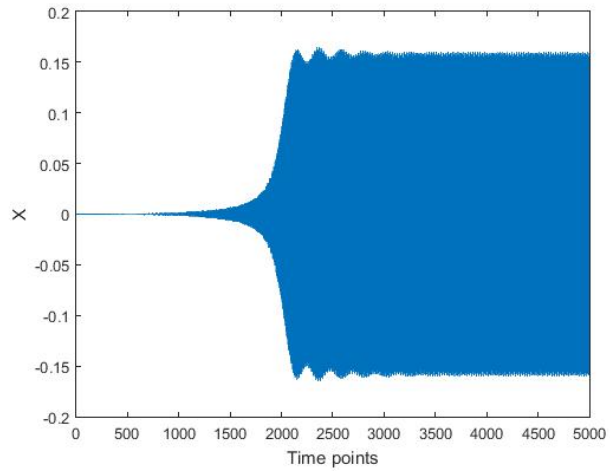


(b)

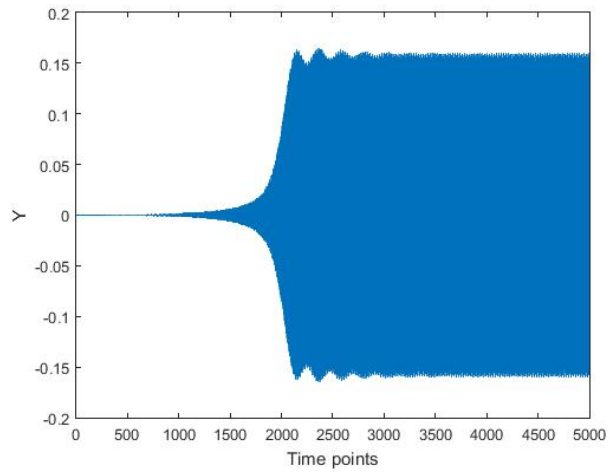


(c)

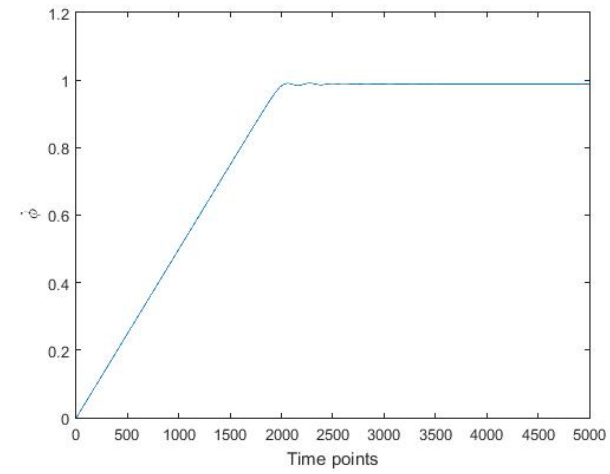
Figure 10: (Passage) X-displacement and y-displacement responses (upper traces) and shaft angular velocity (lower traces) vs. time, as obtained by numerical simulation in search of a passage/capture threshold for the case  $\Omega = 1, \alpha = 0.01, \epsilon = 0.005, M_* = 0.0015$



(a)

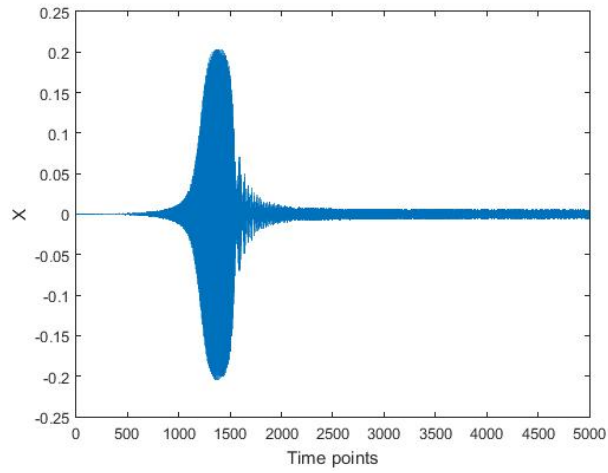


(b)

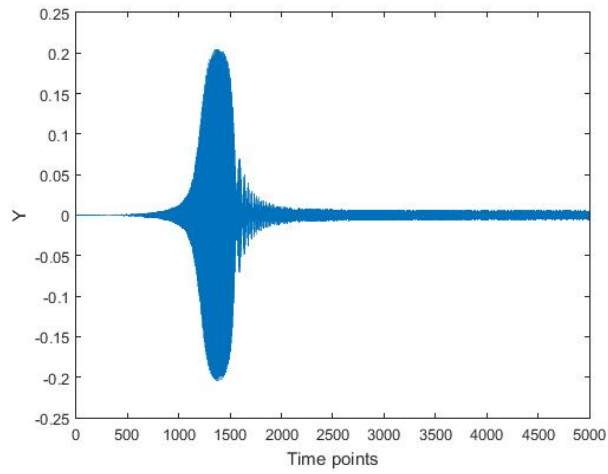


(c)

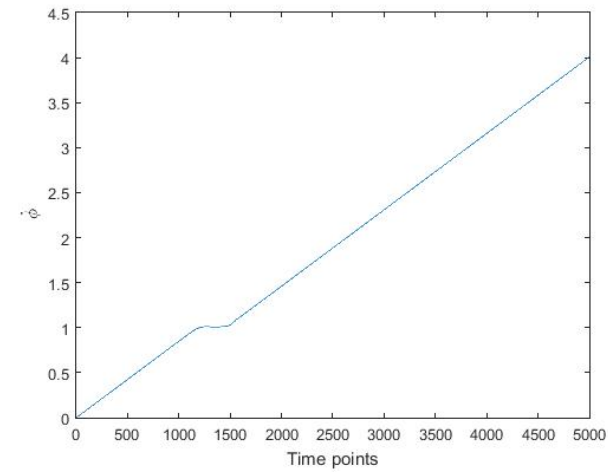
Figure 11: (Capture) X-displacement and y-displacement responses (upper traces) and shaft angular velocity (lower traces) vs. time, as obtained by numerical simulation in search of a passage/capture threshold for the case  $\Omega = 1, \alpha = 0.01, \epsilon = 0.005, M_* = 0.0005$



(a)



(b)



(c)

Figure 12: (Slow-passage) X-displacement and y-displacement responses (upper traces) and shaft angular velocity (lower traces) vs. time, as obtained by numerical simulation in search of a passage/capture threshold for the case  $\Omega = 1, \alpha = 0.01, \epsilon = 0.005, M_* = 0.00085$

## Three cases of motor torque

Based on the plot of steady-state torque  $\bar{M}_{ss}$  vs.  $\nu$ , Figure 5, the curve has peaks at  $\nu = 1$  and  $\nu = \Omega$ . The two extreme values of steady-state torque indicated the technically minimum torque required for x-passage and y-passage, respectively. If the motor torque is above both peaks, passage will occur in both x-axis displacement and y-axis displacement, as shown in Figure 13. The x-displacement reaches its resonance at time point 625, and it passes over the resonance with amplitude returns to a smaller constant value. The y-displacement reaches its resonance at time point 900, and the amplitude returns to a smaller constant value after the passage as well. The angular velocity is increasing throughout the whole process, although it increases at a slower rate during the two passages over x-resonance and y-resonance, which is time points 625 and 900 respectively.

If the value of motor torque is above the first peak at  $\nu = 1$  but below the second peak at  $\nu = \Omega$ , then the x-axis vibration will pass over the x-axis resonance, while y-axis vibration will be captured at y-resonance, as shown in Figure 14. The x-displacement passes over resonance as the previous case, but y-displacement reaches resonance at time point 2000 and is captured with resonant amplitude. Corresponding to x- and y-displacements, the angular velocity increases before the time point 2000 with a slower increasing rate during the passage over x-resonance at the time point 1400, and then it is captured at a constant value around  $\nu = \Omega = 1.5$ , when the y-displacement is captured.

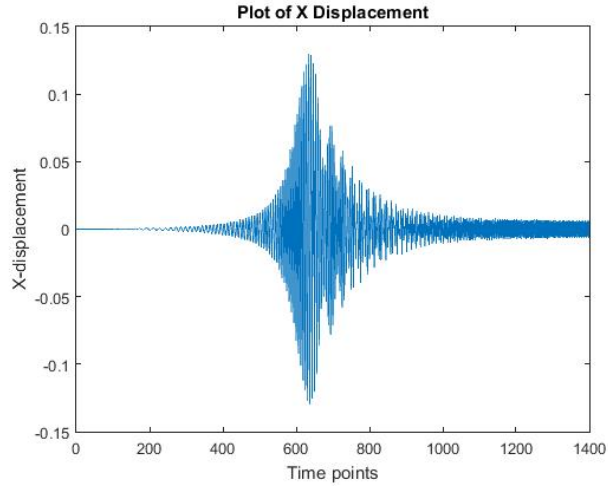
If the motor torque is below both peaks, then both x-displacement and y-displacement will be captured at resonances. The corresponding figure is Figure 15. We can see that both x- and y- displacement have amplitudes maintained at resonance amplitudes after they time they reach resonance. The angular velocity  $\nu$  increases until x-displacement is captured, and it remains constant at 1.

The above three cases of different motor torque are essential to the following process of determining the passage/capture motor torque  $M_*$ .  $(M_*)_1$  denotes the minimum motor

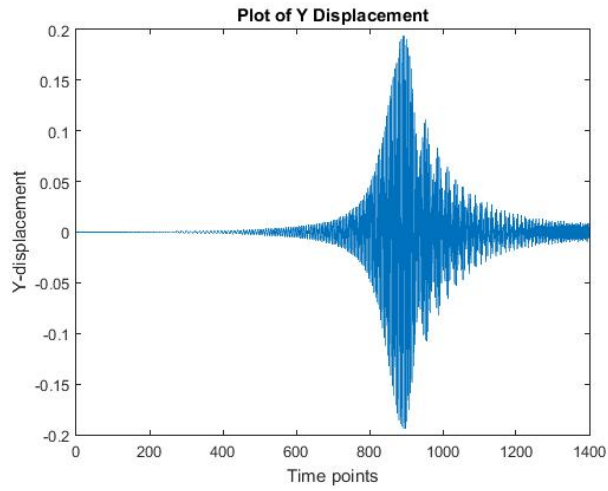
torque required to guarantee a passage over x-resonance, and  $(M_*)_2$  denotes the minimum motor torque required to pass over y-resonance. In the numerical simulation, the value of motor torque  $M_*$  starts from a small value that initially cause capture for both x-vibration and y-vibration, as indicated in the third case, Figure 15. Then the value of  $M_*$  is increased gradually, by the step of  $1 \times 10^{-7}$ .

For axisymmetric case,  $\nu = 1$ , the motor torques required for passage in x-displacement and y-displacement are equal, i.e.  $(M_*)_1 = (M_*)_2$ . So that with a given motor torque  $M_*$ , the x- and y-vibrations will both pass over resonance, or both capture at resonance.

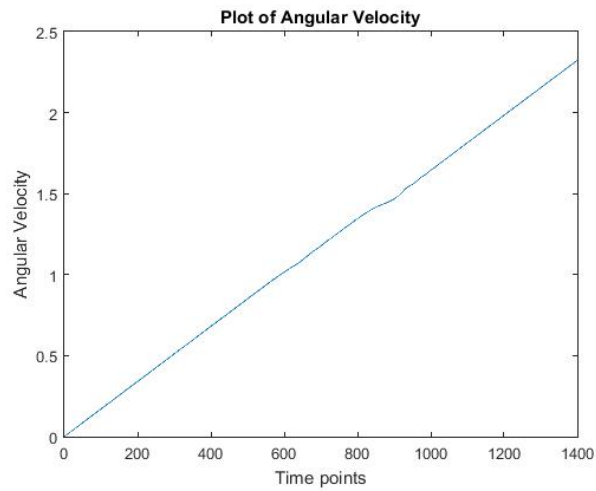
For unsymmetric case that  $\Omega > 1$ , the values of  $(M_*)_1$  and  $(M_*)_2$  are different. From steady-state analysis, we found that  $(M_*)_2$  is always greater than  $(M_*)_1$ , for  $\Omega \geq 1$ . Hence the lowest torque, which allows passage on x-vibration but capture on y-vibration, is the  $(M_*)_1$ . This corresponds to the second case. And in order to find  $(M_*)_2$ , we need to look for the lowest motor required to achieve the first case from the third case, that allows passages on both x-vibration and y-vibration.



(a)

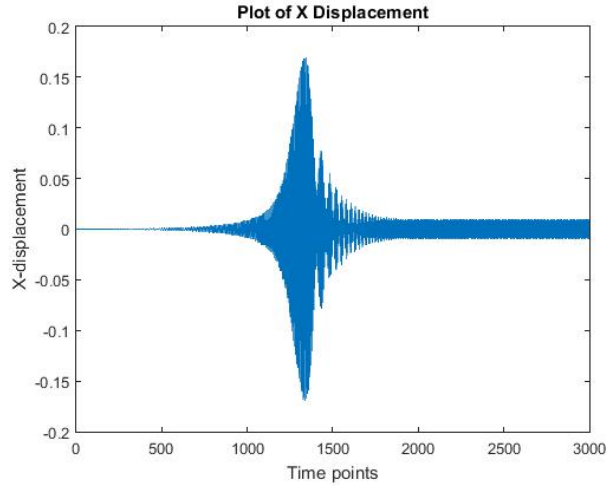


(b)

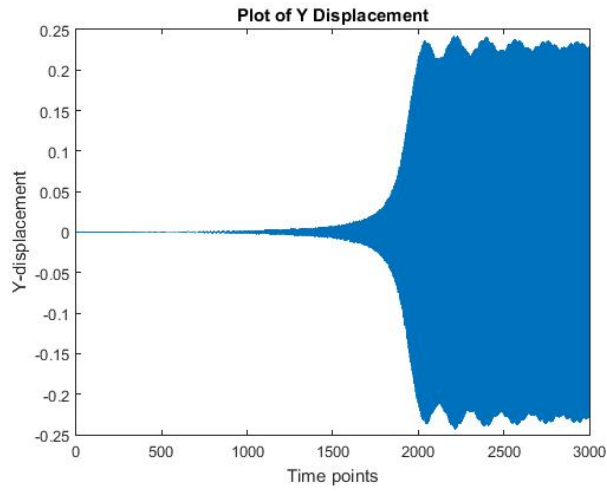


(c)

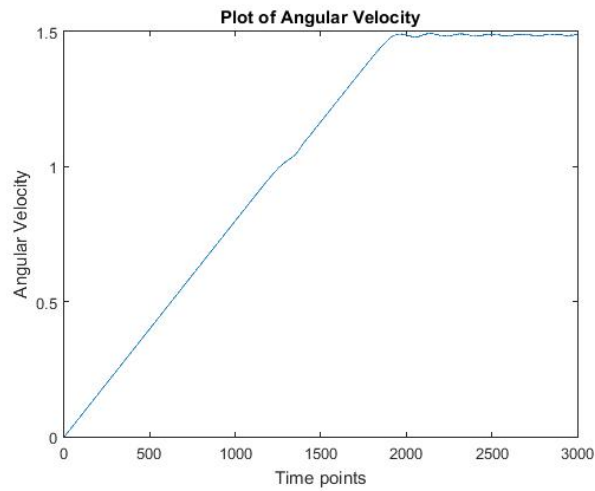
Figure 13: When the motor torque is above both peaks of  $(\bar{M}_{ss})_1$  and  $(\bar{M}_{ss})_2$ , both the x-displacement and y-displacement pass over the resonances with their amplitudes return to smaller constant values. The angular acceleration decreases during x and y resonances, in this case, at time points around 625 and 900.  $\Omega = 1.5, \alpha = 0.01, \epsilon = 0.005, M_* = 0.0012$



(a)

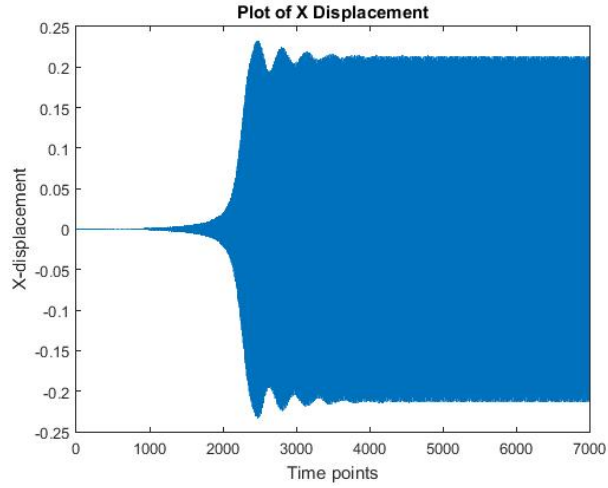


(b)

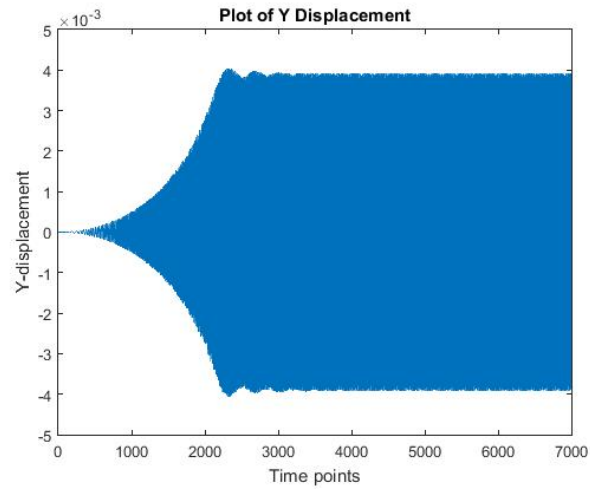


(c)

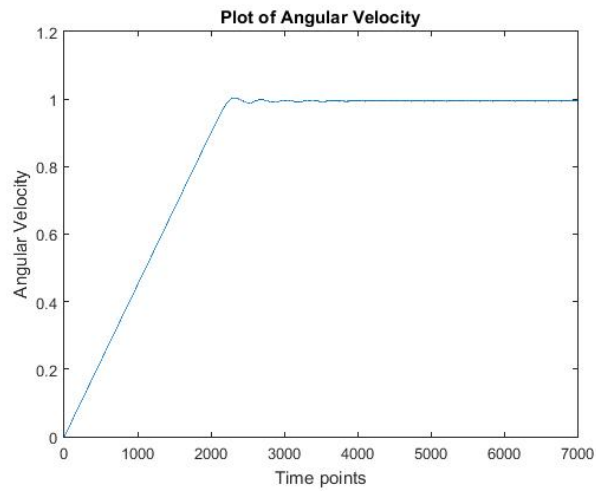
Figure 14: When the motor torque is between the peaks of  $(\bar{M}_{ss})_1$  and  $(\bar{M}_{ss})_2$ , x-axis vibration passes over resonance with amplitude returns to a smaller constant value, while y-displacement is captured at resonance with resonant amplitude. The angular acceleration decreases during the passage in x-displacement at time point around 1400, then it is captured at a constant value around 1.5, starting near the time point when capture occurs in y-displacement.  $\Omega = 1.5, \alpha = 0.01, \epsilon = 0.005, M_* = 0.00085$



(a)



(b)



(c)

Figure 15: When the motor torque is below both peaks of  $(\bar{M}_{ss})_1$  and  $(\bar{M}_{ss})_2$ , both the x-displacement and y-displacement are captured at resonances with large resonant amplitudes. And the angular is captured at a constant value around 1, starting near the time point when capture occurs in x-displacement.  $\Omega = 1.5, \alpha = 0.01, \epsilon = 0.005, M_* = 0.0005$

## Results

### Validation of Steady-state Case

In the numerical simulation, the function of steady-state torque  $\bar{M}_{ss}$  is validated at  $\Omega = 1.2$ . With different initial conditions and motor torque  $M_*$ , the rotation velocity  $\dot{\phi}$  is going to steady-state response. As shown in the figure of  $\bar{M}_{ss}$ , Figure 16, with a given  $M_* = 0.0001$ , then on the horizontal line containing intersections with the curve of steady-state torque  $\bar{M}_{ss}$ , the rotational velocity  $\dot{\phi}$  always goes to the stable steady-state points, as indicated by arrows.

In order to validate the steady-state torque curve  $\bar{M}_{ss}$ , we created Matlab codes to solve the equations of the system, by using Runge-Kutta-Fehlberg method. Starting with the smallest motor torque  $M_* = 0$ , the values of  $M_*$  is gradually increased by the step of  $1 \times 10^{-6}$ . At each value of  $M_*$ , if the initial rotation speed converges to a larger value

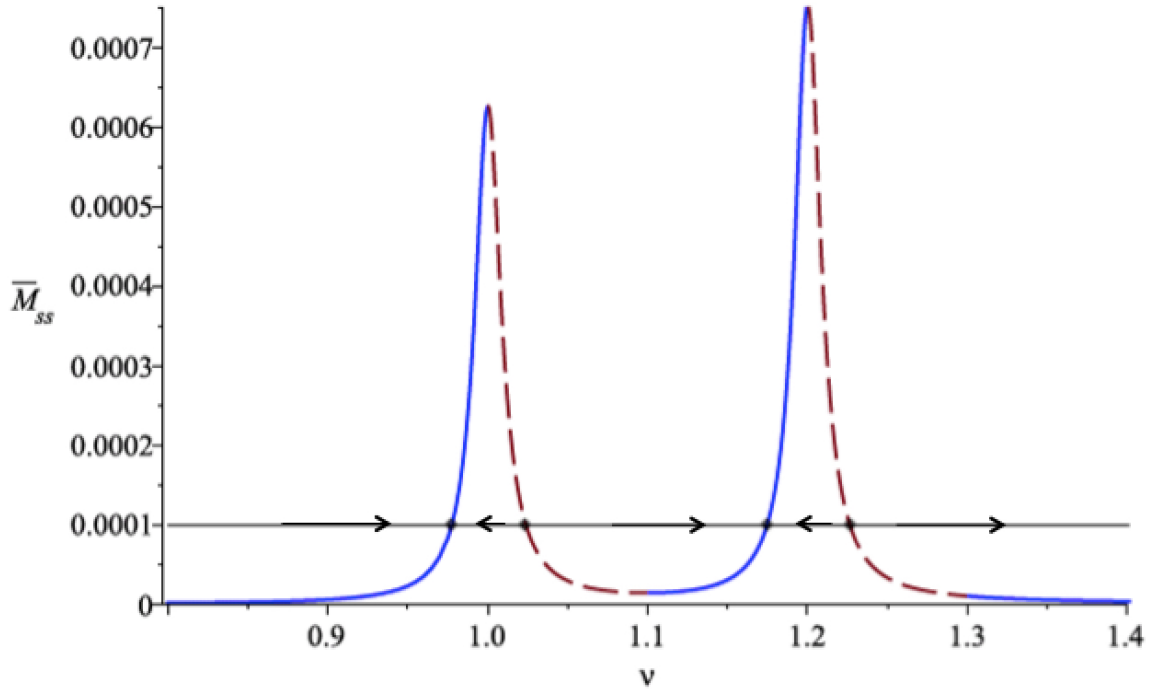


Figure 16: Plot of analytical steady-state threshold torque  $\bar{M}_{ss}$  vs. angular velocity  $\nu$ , with blue curve indicating stable part, and red dashed curve indicating unstable part. The arrows indicates the tendency of solution with specific area of initial conditions

after the process, then the value of convergence is the stable steady-state point. For the initial rotation speed that is near the unstable curves, as plotted in red dashed curve in Fig 16, then the unstable steady-state point is the boundary between increased  $\dot{\phi}$  and decreased  $\dot{\phi}$ . For example, with motor torque  $M_* = 0.00005$ , then when  $\dot{\phi}_0 = 1.041$ , the rotation speed converges to 0.9706. When  $\dot{\phi}_0 = 1.042$ , the rotation speed converges to 1.1563. Then the unstable steady-state point locates between 1.041 and 1.042, which was approximated as 1.0415 in our report.

The curve of  $\bar{M}_{ss}$  plotted by operating numerical simulation is plotted in Figure 17. The blue curve denotes the stable part of the steady-state torque, and the red dashed curve denotes the unstable part of the steady-state torque. The curve of  $\bar{M}_{ss}$  from numerical simulation has the same shape with the curve of the analytical steady-state torque function, Figure 9, and the coordinates of points on the curves match each other. Therefore, the numerical simulation validates the analytical result of steady-state torque function  $\bar{M}_{ss}$ .

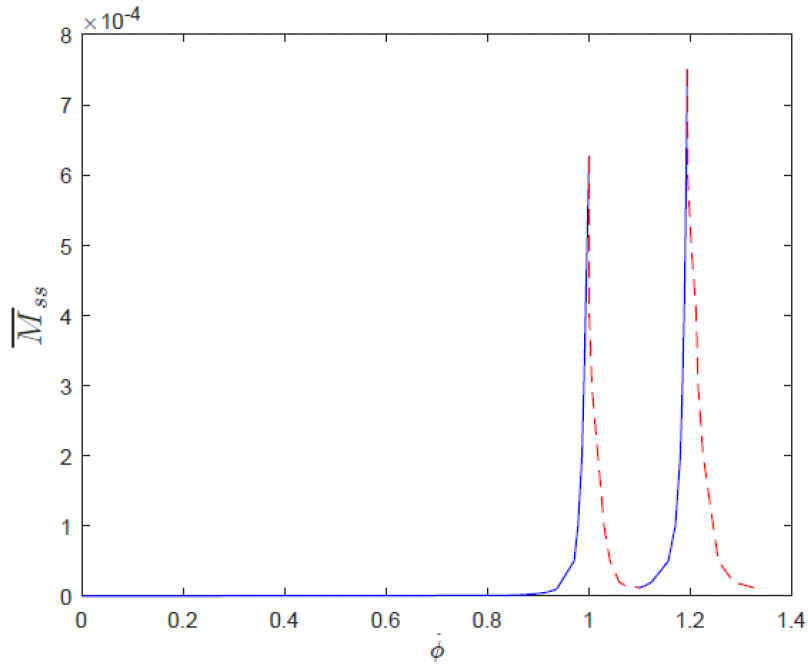


Figure 17: Plot of numerical steady-state threshold torque  $\bar{M}_{ss}$  vs. angular velocity  $\nu$ , with blue curve indicating stable part, and red dashed curve indicating unstable part.

Figure 17 also validate the stability criteria of steady-state response, which was discussed under the Transient Response section. From the analytical analysis, positive  $\beta$  indicates stable steady-state response, and negative  $\beta$  indicates unstable steady-state response. Since with the initial rotation speed, which already allows both passages for  $x$ -vibration and  $y$ -vibration, the rotation speed  $\dot{\phi}$  will keep increasing until an extremely large value at stable steady-state, we do not consider the part of function  $\bar{M}_{ss}$  that has  $\nu > 2$ . For the case  $\alpha = 0.01$ ,  $\epsilon = 0.005$ , and  $\Omega = 1.2$ , the stable steady-state is in the intervals of  $\nu$ :  $[0, 1]$  and  $[1.1, 1.2]$ , and unstable steady-state is in the intervals:  $(1, 1.1)$  and  $(1.2, 2]$ . From the numerical simulation, the stable steady-state is in the intervals of  $\nu$ :  $[0, 0.993]$  and  $[1.1113, 1.193]$ . When  $M_* = 0.0005$ ,  $x$ -vibration occurs “slow passage” over resonance, which exists in practical vibration systems, but is not considered in the analytical analysis of steady-state response. The “slow passage” obstructs the searching of stable steady state because it allows rotation speed to increase at the point where should be captured at stable steady-state technically. Similarly, for  $\nu > 1.193$ , “slow passage” occurs in  $y$ -vibration, and the stable steady-state cannot be determined. Also, since the values of  $\nu$  in numerical simulation are discrete points, some information is lost between adjacent points with the difference as 0.001. The unstable steady-state is in the intervals:  $[1, 1.1]$  and  $[1.18, 1, 133]$ . Due to the error of estimation in numerical simulation, we are not able to obtain the stability criteria for the interval  $[1.134, 2]$ , so the stability criteria for  $\bar{M}_{ss}$  in numerical simulation was only considered in  $0 \leq \nu \leq 1.133$ .

Despite the limitation of numerical simulation, the  $\bar{M}_{ss}$  curve obtained numerically matches the analytical steady-state torque curve  $\bar{M}_{ss}$ . Therefore, the analytical function of  $\bar{M}_{ss}$ , as well as its stability criteria, is validated by numerical simulation.

### Passage Technique for Axisymmetric Case

In order to verify the hypothesis of passage technique for axisymmetric vibration system, which is discussed in Steady-state Response section, we need numerical simula-

tion to validate the functions of steady-state torque at  $\nu = 1$ ,  $(\bar{M}_{ss})_1$  with Eq (51), and steady-state torque at  $\nu = \Omega$ ,  $(\bar{M}_{ss})_2$  with Eq (52).

The  $\bar{M}_{ss}$  value at two peaks at  $\nu = 1$  and  $\nu = \Omega$  are used as reference points of starting values of real threshold torque for dynamic passage. A motor torque that is slightly below the curve  $\bar{M}_{ss}$  is the starting point of  $M_*$ , which means this initial value of motor torque guarantees capture on both  $x$ -displacement and  $y$ -displacement. The value of this starting point is 0.0005. Then raise the value of motor torque gradually, by the step of  $1 \times 10^{-7}$ , until passage firstly occurs. This real threshold of dynamic passage,  $M_*$  will be recorded and compared with the steady-state torque  $\bar{M}_{ss}$  at different values  $\Omega$ .

#### a. Passage on $x$ -displacement but capture on $y$ -displacement

To look for the peak values of threshold torque at  $\nu = 1$ , the second case discussed in the Three cases of motor torque is the case under consideration. In this case, we need to find the numerical threshold motor torque that allows passage on  $x$ -axis vibration, but with  $y$ -axis vibration captured at  $y$ -resonance. Also, in the figure of function  $\bar{M}_{ss}$ , Figure 5, this case indicates the motor torque that is above the first peak at  $\nu = 1$  and below the second peak at  $\nu = \Omega$ . The only output of this case is that  $x$ -passage and  $y$ -capture occur simultaneously.

By raising the value of  $\Omega$ , and use the above method to find numerical threshold motor torque of dynamic passage on  $x$ -displacement, and capture on  $y$ -displacement simultaneously, we collected the data of  $(M_*)_1$  with respect to  $\Omega$  in Table 1 in Appendix A.

#### b. Passage on both $x$ -displacement and $y$ -displacement

The case of passage on both  $x$ -displacement and  $y$ -displacement corresponds to the first case of the three cases of motor torque as described in previous section. In this case, the motor torque should be large enough to allow both passages over  $x$ -resonance and

$y$ -resonance. Since torque required to pass over  $y$ -resonance is greater than the torque required to pass over  $x$ -resonance, the passage on  $y$ -displacement guarantees the passage on  $x$ -displacement.

By raising the value of  $\Omega$ , and use the above method to find numerical threshold motor torque of dynamic passage on  $y$ -displacement, we collected the data of  $(M_*)_2$  of passage on both  $x$ - and  $y$ -displacements with respect to  $\Omega$ . The values of numerical threshold  $(M_*)_2$  can be found in Table 1 in Appendix A as well.

### c. Comparison

With the collected values of  $(M_*)_1$  and  $(M_*)_2$  at different  $\Omega$ , we make a comparison between the numerical threshold torques and analytical threshold torques. Figure 18 demonstrates  $(\bar{M}_{ss})_1$  and  $(M_*)_1$  versus  $\Omega$ . The two curves match except for ratio of stiffness that is very close to 1. This figure shows that the tendency of real threshold motor torque  $M_*$  for passage on  $x$ -displacement and capture on  $y$ -displacement is the same as the analytical threshold  $\bar{M}(\nu_1)$ , which have high value at  $\Omega = 1$ , decreases

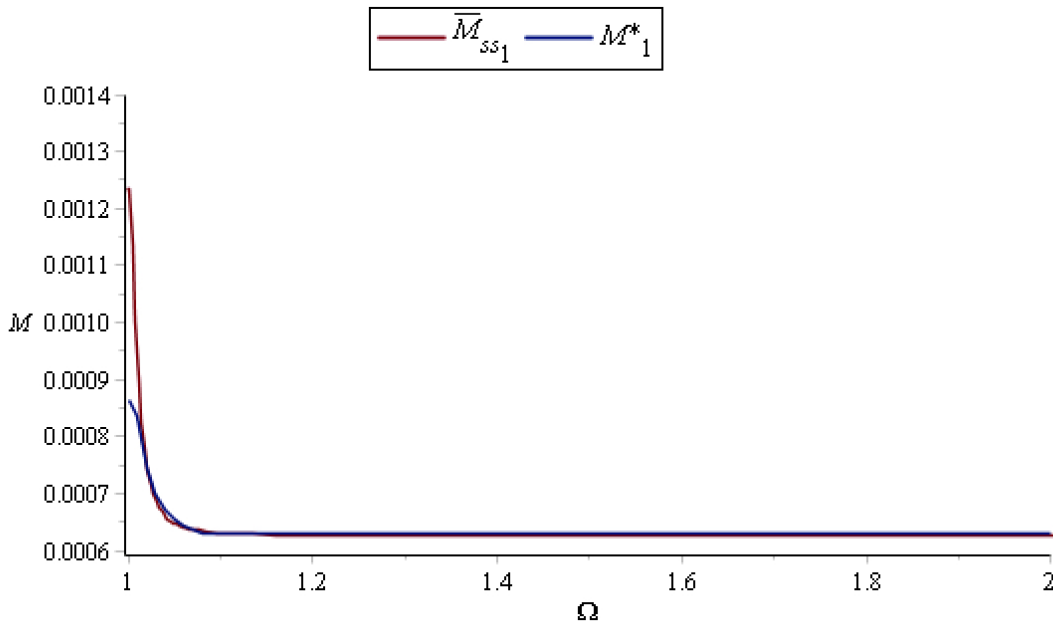


Figure 18: Plot of analytical steady-state threshold torque at  $\nu = 1$ ,  $(\bar{M}_{ss})_1$  in red, and numerical steady-state threshold torque at  $\nu = 1$ ,  $(M_*)_1$  in blue, vs.  $\Omega$ .

rapidly in ratio 1 to 1.05, and remains at a constant value.

Next, we plot  $(\bar{M}_{ss})_2$  and  $(M_*)_2$  versus  $\Omega$ , as shown in Figure 19. The blue curve shows  $(\bar{M}_{ss})_y$ , which decreases in the range of ratio of stiffness 1 to 1.03, and then increases with increasing ratio of stiffness. However, the red curve of  $M_*$  does not have an obvious decrease with small ratio of stiffness, although it increases for large ratio as  $(\bar{M}_{ss})_2$  does. Also, the increasing rate of  $M_*$  for large  $\Omega$  is much smaller than the increasing rate for  $(\bar{M}_{ss})_2$ , which is due to the specific condition (small difference of stiffnesses) applied in the analytical analysis.

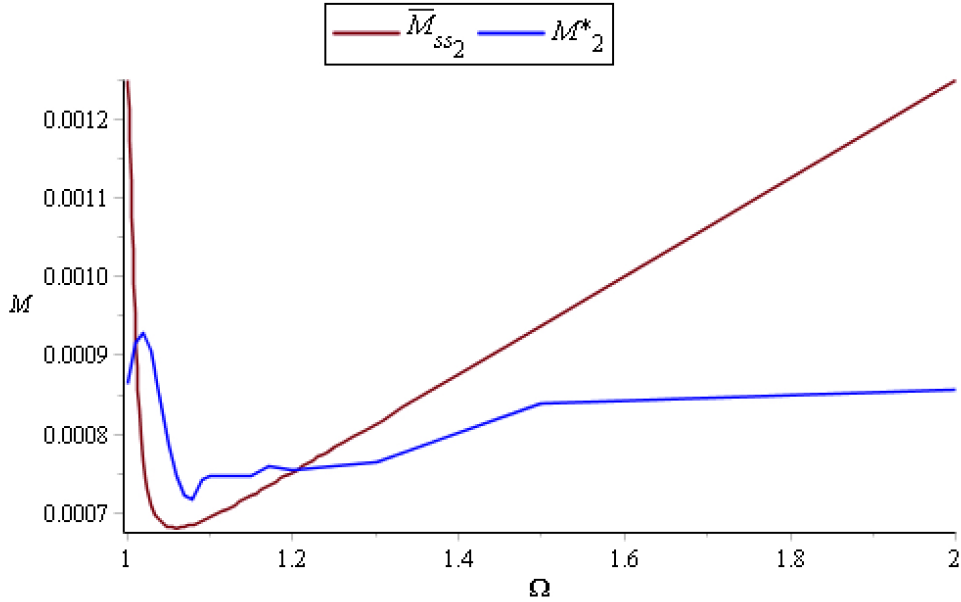


Figure 19: Plot of analytical steady-state threshold torque at  $\nu = \Omega$ ,  $(\bar{M}_{ss})_2$  in red, and numerical steady-state threshold torque at  $\nu = \Omega$ ,  $(M_*)_2$  in blue, vs.  $\Omega$ .

The graph of analytical threshold  $\bar{M}_{ss}$  at two peaks is also plotted as in Figure 20. From this figure, we can see if we start with an axisymmetric stiffnesses system, the motor torque required for passage on both x-displacement and y-displacement can be reduced by increasing the ratio of stiffness to 1.3. This leads to a technique of passage, which is when we have the axisymmetric case which vibrations are captured at both x-resonance and y-resonance, we can raise one of the stiffness slightly with additional stiffness to achieve passage.

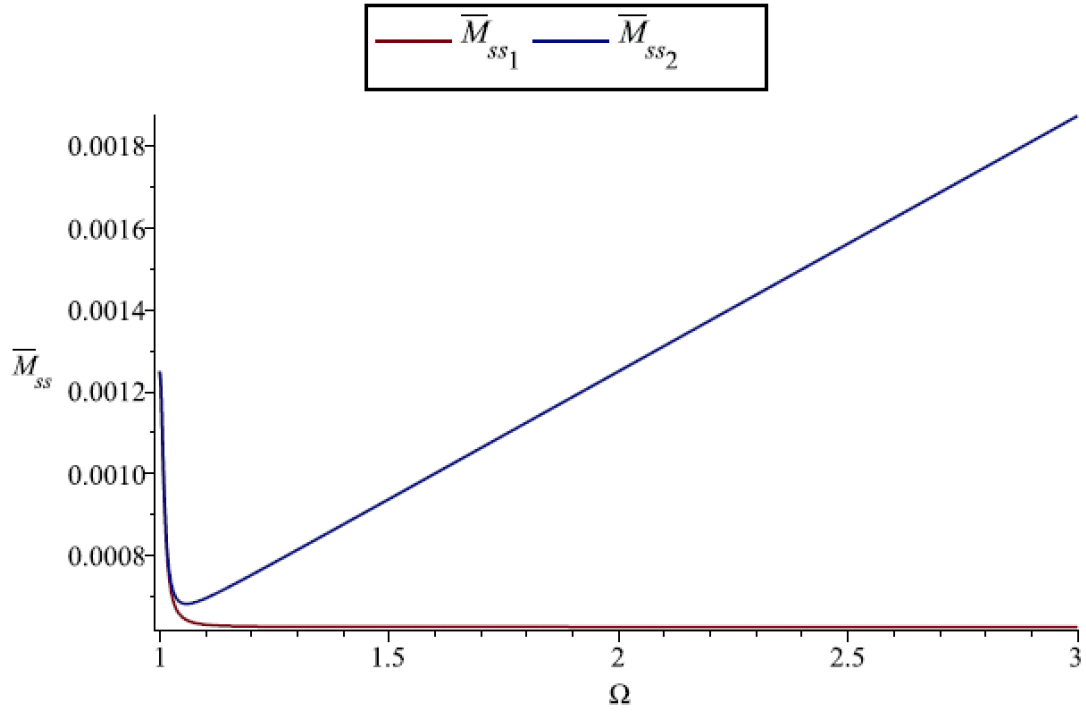


Figure 20: Plot of analytical steady-state threshold torque at  $\nu = 1$ ,  $(\bar{M}_{ss})_1$  in red, and analytical steady-state threshold torque at  $\nu = \Omega$ ,  $(\bar{M}_{ss})_2$  in blue, vs.  $\Omega$ .

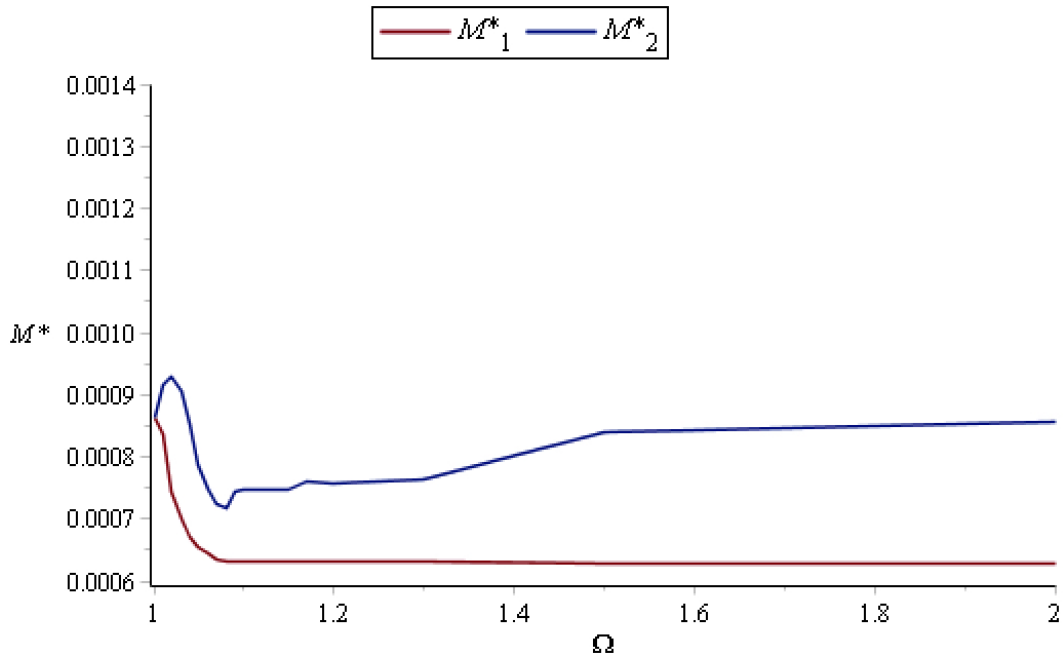


Figure 21: Plot of numerical steady-state threshold torque at  $\nu = 1$ ,  $(M^*)_1$  in red, and numerical steady-state threshold torque at  $\nu = \Omega$ ,  $(M^*)_2$  in blue, vs.  $\Omega$ .

We also plot the figure of numerical threshold  $(M_*)_1$  and  $(M_*)_2$  versus  $\Omega$  as Figure 21. From this graph, we can see although the decrease of motor torque required for passage is small, it is still lower than the motor torque of passage in axisymmetric case. The two Figures 20 and 21 are generally similar to each other, which shows that the analytical results correctly demonstrate the real situation of 2D vibration.

## 7 Conclusion

In this report, we deal with a two-dimensional vibration system, with two spring sets attached to the unbalanced shaft. The two extreme cases: axisymmetric case where the ratio of spring stiffness is 1; one-dimensional case where the ratio of spring stiffness is infinity, are considered, as well as the cases in between. In the first half of the report, we introduce the analytical method: Krylov-Bogoliubov Averaging method to solve for steady-state case and transient case. We also consider the stability criteria for steady-state case. By considering the two peaks of steady-state torque curve  $\bar{M}_{ss}$ , we come up with a hypothesis of passage technique for axisymmetric vibration system.

In the second half of the report, we use numerical simulation to validate the analytical results. The numerical method used is Runge-Kutta-Fehlberg method. The numerical simulation validates the steady-state curve of torque  $\bar{M}_{ss}$ , and its stability criteria. Then the values of real threshold torque at two specific points:  $(M_*)_1$  at  $\nu = 1$ , and  $(M_*)_2$  at  $\nu = \Omega$ , are collected and plotted. By comparing these two figures with the figures of steady-state torque at those two points,  $(\bar{M}_{ss})_1$  at  $\nu = 1$ , and  $(\bar{M}_{ss})_2$ , we find that the hypothesis of passage technique for axisymmetric vibration system is supported by the numerical results. Therefore, with a constant motor torque  $M_*$  applying to an axisymmetric vibration system, which firstly makes vibrations be captured at resonance, can passage over the resonances by raising the spring stiffness of one of the spring set. Raising the system stiffnesses is possible through accounting finite stiffnesses of the bearing support, by adding an additional spring set to the original spring set. The stiffnesses  $K$  has the relation  $\frac{1}{K} = \frac{1}{K_{shaft}} + \frac{1}{K_{bear}}$ , where the bear stiffnesses  $K_{bear}$  are different in  $x$ - and  $y$ - directions after adding extra spring set. We are able to calculate the splitted stiffness by substituting the new  $K_{bear}$  into the relation.

For plants and machinery with axisymmetric support stiffness, which require using motor to accelerate the rotation of shaft, the passage technique introduced in the report allows a lower power supply required to pass over the resonances. The motor torque is

always nonlinear, which decreases at higher rotation velocity  $\dot{\phi}$ , although only constant motor torque is considered in the report, the result applies to nonlinear motor torque as well. By substituting the threshold steady-state torque  $\bar{M}_{s,s}$  into the nonlinear motor torque function, we are able to find the initial motor torque required for passage. With the passage technique, axisymmetric vibrating system can save power supply on passing over resonance, also reduces the time of passing over resonance with high resonant amplitude. This is essential to machine life because the high amplitude of vibration can destroy the supporting foundation. Although simply using all driving power available to achieve a quick passage over resonance is a way to prevent capture at resonance, the large amplitude of vibration at resonance is still a concern. By adding extra spring to one of the spring set, resonance is passed over in a shorter time with smaller amplitude. The technique saves energy input and extends machine life.

In a broader analysis, we may include nonlinearity in the two-dimensional vibration system, such as nonlinear motor torque function, and nonlinear stiffness support. In real life applications, the motor torque is always nonlinear, and it decreases at higher rotation speed. The nonlinear stiffness of spring with different materials, for example, copper, aluminum, and ceramic materials, are introduced at the beginning of the report. For specific plants and machinery, the nonlinearity of stiffness needs to be considered based on the material of support.

## 8 Appendices

### Appendix A: Table of analytical steady-state torque $\bar{M}_{ss}$ and numerical steady-state torque $M_*$ at $\nu = 1$ and $\nu = \Omega$

With different ratio of stiffness  $\Omega_y/\Omega_x$ , we collected the following data of analytical threshold of passage on x-displacement but capture on y-displacement, denoted as  $\bar{M}(\nu_1)$  of passage on both x- and y-displacements, denoted as  $\bar{M}(\nu_2)$ . Also, the values of numerical threshold of passage on x-displacement but capture on y-displacement,  $(M_*)_x$ , and of passage on both x- and y-displacements,  $(M_*)_y$ , are demonstrated in the table as well.

$\Omega_y/\Omega_x$	$(\bar{M}_{ss})_1$	$(M_*)_1$	$(\bar{M}_{ss})_2$	$(M_*)_2$
1	0.0012500	0.0008634	0.0012500	0.0008634
1.01	0.0009359	0.0008366	0.0009484	0.0009165
1.02	0.0007480	0.0007446	0.0007670	0.0009294
1.03	0.0006858	0.0007002	0.0007098	0.0009059
1.04	0.0006604	0.0006706	0.0006896	0.0008523
1.05	0.0006479	0.0006530	0.0006827	0.0007866
1.06	0.0006409	0.0006451	0.0006814	0.0007482
1.07	0.0006367	0.0006350	0.0006830	0.0007235
1.08	0.0006339	0.0006300	0.0006862	0.0007173
1.09	0.0006320	0.0006300	0.0006903	0.0007434
1.10	0.0006306	0.0006310	0.0006949	0.0007483
1.15	0.0006274	0.0006301	0.0007224	0.0007474
1.17	0.0006268	0.0006301	0.0007342	0.0007590
1.20	0.0006263	0.0006301	0.0007522	0.0007556
1.30	0.0006255	0.0006301	0.0008136	0.0007639
1.50	0.0006252	0.0006290	0.0009380	0.0008400
2.00	0.0006250	0.0006292	0.0012502	0.0008555

Table 1: Table of analytical steady-state threshold torque  $(\bar{M}_{ss})_1$  at  $\nu = 1$ , and  $(\bar{M}_{ss})_2$  at  $\nu = \Omega$ , numerical steady-state threshold torque  $(M_*)_1$  at  $\nu = 1$ , and  $(M_*)_2$  at  $\nu = \Omega$ , with different values of  $\Omega$

## Appendix B: Matlab codes

### a. Equations of system

```
function f = f(t, x0,pars,gamma,perc,M)

% Two-dimensioanl vibration governing equations
% Date: 11/16/2015. Author:Jiaxun Xie

%% Initial Conditions
%x0(1) = x0;
%x0(2) = v0;    %v0 = dx/dt
%x0(3) = y0;
%x0(4) = u0;    %u0 = dy/dt
%x0(5) = phi0;
%x0(6) = nu0;   %nu = d(phi)/dt
%pars = [omega_y/omega_x, alpha/omega_x, epsilon]

%%NONDIMENSIONAL
% Nondimensionalized by tau=(omega_x)*t
% Omega_x = 1

A = x0(2); %v
B = pars(3)*(x0(6)^2)*cos(x0(5))-2*pars(2)*x0(2)-x0(1); %vdot
C = x0(4); %u
D = pars(3)*(x0(6)^2)*sin(x0(5))-2*pars(2)*x0(4)-(pars(1)^2)*x0(3); %udot
E = x0(6); %nu
F = M + pars(3)*(B*sin(x0(5))-D*cos(x0(5))); %nudot

f = [A;B;C;D;E;F];
end
```

## b. Runge-Kutta-Fehlberg method

```
function [X, T] = rkf(f, a, b, x0, tol, hmax, hmin, pars, gamma, perc, M)

%Input:
% endpoints, a and b
% initial condition, x0
% tolerance, tol
% maximum and minimum step size, hmax and hmin

%Output:
% approximation of X(t), x
% step size, h

t = a;
x = x0;
h = hmax;
flag = 1;
X = x0;
T = a;

while (flag==1)
    k1 = h*feval(f, t, x, pars, gamma, perc, M);
    k2 = h*feval(f, t+1/4*h, x+1/4*k1, pars, gamma, perc, M);
    k3 = h*feval(f, t+3/8*h, x+3/32*k1+9/32*k2, pars, gamma, perc, M);
    k4 = h*feval(f, t+12/13*h, x+1932/2197*k1-7200/2197*k2+7296/2197*k3, pars, gamma, perc, M);
    k5 = h*feval(f, t+h, x+439/216*k1-8*k2+3680/513*k3-845/4104*k4, pars, gamma, perc, M);
    k6 = h*feval(f, t+1/2*h, x-8/27*k1+2*k2-3544/2565*k3+1849/4104*k4-11/40*k5, pars, gamma, perc, M);

    R = (1/h)*abs(1/360*k1 - 128/4275*k3 - 2197/75240*k4 + 1/50*k5 + 2/55*k6);

    %error
```

```

if norm(R)<=tol
t = t+h;      % Approximately accepted time step
x = x + 25/216*k1 + 1408/2565*k3 + 2197/4104*k4 - 1/5*k5;
X = [X x];
T = [T t];%Output

%Calculate new h
delta = 0.84*(tol./R).^(1/4);
%Case 1 smaller than minimum, decrease step size
if norm(delta) <= 0.1
    h=0.1*h;
else
%Case 2 greater than maximum, increase step size
    if norm(delta) >= 4
        h = 2*h;

%Case 3 error within max and min, keep the step size
    else
        h = norm(delta)*h;
    end
end
else
    h = 0.5*h;
end
if h >= hmax
    h = hmax;
else h=h;
end

if t>=b
    flag = 0;
else

```

```

        if t+h>b
            h = b-t;
        else
            if h<hmin
                flag = 0;
            end
        end
    end
end
end
end

```

### c. Simulation by RKF

```

%% Inputs:
a = 0;
b =3000;
%x = [x,dx/dt, y,dy/dt, phi,nu)
x0 = [0;0;0;0;0;0];
tol = 1e-4;
hmax = 1;
hmin = 0.1;
gamma=0;perc=0;
%pars = [omega_y/omega_x, alpha/omega_x, epsilon]
%omega_x is assumed to be 1, so that pars = [omega_y, alpha, epsilon]
pars = [1.2;0.01;0.005];
M = 0.0011
M_x = (pars(3)^2/(4*pars(2)*(1+pars(3)^2)))*(1+1/(1+(pars(1)^4 - 2*pars(1)^2+1)/(4*pars(2)
M_y = pars(2)*pars(3)^2*pars(1)^3/(1+pars(3)^2)*(1/((1-pars(1)^2)^2+4*pars(2)^2*pars(1)^2
    1/(4*pars(2)^2*pars(1)^2))
%f_y = M - 600000^(-1)*integral(@M_y,0,600000)

%% RKF

```

```

f1=@f;
[X, T] = rkf(f1, a, b, x0, tol, hmax, hmin, pars, gamma, perc, M);
% [X,T]=findm(rkf, a, b, x0, tol, hmax, hmin, pars, gamma, perc, M1)

%% Check passage/capture
%Check y-passage/capture
checkY = X(6, X(6,:) > pars(1) - 0.1);
G_y = gradient(checkY);
if any(G_y < 0)
    'y-capture'
else 'y-passage'
end
%For r > 1.1, checkY > pars(1) - 0.1
%For r <= 1.1, checkY > pars(1) - 0.01

%Check x-passage/capture
checkX = X(6, X(6,:) >= 0.99 & X(6,:) <= 1.01);
G_x = gradient(checkX);
if any(G_x < 0)
    'x-capture'
else 'x-passage'
end

%% Plots
figure(1)
%plot of x displacement
plot(T, X(1,:))
xlabel('Time points'), ylabel('X')

figure(2)
%plot of y displacement
plot(T, X(3,:))
xlabel('Time points'), ylabel('Y')

```

```
figure(3)
% plot of angular velocity
plot(T, X(6,:))
xlabel('Time points'), ylabel('$\dot{\phi}$', 'Interpreter', 'latex')
dnu = diff(X(6,:))./diff(T);
```

## References

- [1] Sommerfeld, A., Beitrage zum dynamischen Ausbau der Festigkeitslehre, Physikalische Zeitschrift, 1902, 12, 13 [in German].
- [2] Kinsey, R.j., D.l. Mingori, and R.h. Rand. "Nonlinear Controller to Reduce Resonance Effects during Despin of a Dual-spin Spacecraft through Precession Phase Lock." [1992] Proceedings of the 31st IEEE Conference on Decision and Control (1992): n. pag. Web.
- [3] M.F. Dimentberg, L. McGovern, R.L. Norton, J. Chapdelaine, R. Harrison, Dynamics of an unbalanced shaft interacting with a limited power supply, Nonlinear Dyn., 13 (1997), pp. 171187.
- [4] Segalman, D. J., Parker, G. G., and Inman, D. J., 1993, "Vibration Suppression by Modulation of Elastic Modulus Using Shape Memory Alloy," Intelligent Structures, Materials, and Vibrations, M. Shahinpoor and H. S. Tzou (Eds.), DE-Vol. 58, ASME, New York
- [5] Kononenko, V.O., Korablev, S.S., 1959. An experimental investigation of the resonance phenomena with a centrifugal excited alternating force. Tr. Mosk. Tek. Instutita 14, 224232.
- [6] Cveticanin, L., and M. Zukovic. "Motion of a Motor-structure Non-ideal System." European Journal of Mechanics - A/Solids 53: 229-40.
- [7] Samantaray, A.k., S.s. Dasgupta, and R. Bhattacharyya. "Sommerfeld Effect in Rotationally Symmetric Planar Dynamical Systems." International Journal of Engineering Science 48.1 (2010): 21-36.
- [8] Tsui, Raymond, and Christopher Hall. "Resonance Capture in Unbalanced Dual-spin Spacecraft." Astrodynamics Conference (1994): n. pag. Web.

- [9] Verhulst, Ferdinand. "Profits and Pitfalls of Timescales in Asymptotics." *SIAM Rev.* *SIAM Review* 57.2 (2015): 255-74. Web.
- [10] Bolla, M. R., J. M. Balthazar, J. L. P. Felix, and D. T. Mook. "On an Approximate Analytical Solution to a Nonlinear Vibrating Problem, Excited by a Nonideal Motor." *Nonlinear Dynamics Nonlinear Dyn* 50.4 (2007): 841-47. Web.
- [11] Prathap, G., Varadan, T.K., 1976. The inelastic large deformation of beams. *ASME J. Appl. Mech.* 43, 689-690.
- [12] Lo, C.C., Gupta, S.D., 1978. Bending of a nonlinear rectangular beam in large deflection. *J. Appl. Mech. ASME* 45, 213-215.
- [13] Colm, I.J., Clark, N.J., 1988. *Forming, Shaping and Working of High-performance Ceramics*. Blackie, New York.
- [14] Perturbation theory. N.N. Bogolyubov, jr. (originator), *Encyclopedia of Mathematics*.
- [15] Marinca, Vasile, and Nicolae Herisanu. "Perturbation Method: Lindstedt-Poincar." *Nonlinear Dynamical Systems in Engineering: Some Approximate Approaches*. Berlin: Springer, 2011. 9-29. Print.
- [16] KrylovBogolyubov method of averaging. *Encyclopedia of Mathematics*.
- [17] Burden, Richard L., J. Douglas Faires, and Annette M. Burden. *Numerical Analysis*. N.p.: n.p., n.d. Print.
- [18] Kononenko, Viktor Olimpanovich. *Vibrating Systems with a Limited Power Supply*. London: Iliffe, 1969. Print.